# Chapter 4 Linear Wave Theory

## 4.1 Introduction and Classification of Wave Types

One of the most important dynamical properties of the atmosphere is its ability to support wave motions. These waves are of many different types, and in this chapter we shall concentrate on those that are of greatest importance for the large-scale behavior of the middle atmosphere. Thus we shall exclude discussion of acoustic waves, which have frequencies comparable to or larger than the buoyancy frequency and violate the hydrostatic relation of Eq. (3.1.3c); we shall also omit reference to waves modified by electrodynamic effects, which are important in the thermosphere.

The restoring effects necessary for the existence of the waves to be considered here are provided by the stable density or entropy *stratification* of the atmosphere, as represented by positive values of $N^2$ or $\theta_{0z}$, and by the *rotation* of the earth, as represented by the Coriolis parameter $f = 2\Omega \sin \phi$ and its latitudinal derivative $\beta = 2\Omega a^{-1} \cos \phi$ (cf. Section 3.2).

In this chapter we shall concentrate exclusively on *linear* waves, assumed to be of small enough amplitude for the equations of Section 3.4 to apply. Even in this linear case, it is difficult to formulate a precise definition of a "wave"—indeed, no one definition is likely to satisfy all meteorologists. However, some sort of quasi periodicity is usually implied by the term, as well as the ability to transfer "information" over large distances without the corresponding transport of fluid parcels: all the waves to be discussed here possess these two attributes.[1]

Atmospheric waves can be classified in various ways, according to their physical or geometrical properties. In the first place, they can be categorized

[1] Incidentally, the departure from the zonal mean, defined by Eq. (3.3.1b), or any of its zonal Fourier components, is often called a "wave," despite the fact that it need not generally be "wave-like" in form.

according to their restoring mechanisms: thus buoyancy, or internal gravity, waves (often called "gravity waves" for short) owe their existence to stratification, while inertio-gravity waves result from a combination of stratification and Coriolis effects. Planetary, or Rossby, waves result from the beta-effect or, more generally, from the northward potential vorticity gradient [Eq. (3.4.8)].

A second type of classification is to distinguish *forced* waves, which must continually be maintained by an excitation mechanism of given phase speed and wave number, from *free* waves, which are not so maintained. Examples of forced waves include thermal tides, which are induced by the diurnal fluctuations in solar heating (see Section 4.3), while examples of free waves include global normal modes (Section 4.4).

A further classification results from the fact that some waves can propagate in all directions, while others may be trapped (or evanescent) in some directions. Thus under some circumstances horizontally propagating planetary waves can be trapped in the vertical (Section 4.5), while equatorial waves can propagate vertically and zonally but are evanescent with increasing distance from the equator (Section 4.7).

Waves can also be separated into *stationary* waves, whose surfaces of constant phase are fixed with respect to the earth, and *traveling* waves, whose phase surfaces move. Since information propagates with the group velocity (Section 4.5) and not with the phase speed, propagation can still occur in stationary waves. (We here use the adjective "steady" to denote waves whose amplitudes are independent of time, and "transient" for waves whose amplitudes are time-varying; see Section 3.6. Some authors use these terms as synonyms for our "stationary" and "traveling," while another definition of "transient" is mentioned in Section 5.1. What we have called stationary waves are sometimes also known as standing waves; however, the latter name is best reserved for waves with fixed nodal surfaces as typified, say, by a velocity disturbance $u' \propto \cos kx \cos \omega t$.)

The final general form of classification that we shall mention distinguishes waves that do not lead to any mean-flow acceleration from those that do. The former category includes waves that are linear, steady, frictionless, and adiabatic (see Section 3.6), while the latter usually includes any wave that is transient or nonconservative; however, nonlinear waves can sometimes satisfy nonacceleration conditions if they are steady and conservative.

## 4.2 Wave Disturbances to a Resting Spherical Atmosphere

When a stratified spherical atmosphere, at rest with respect to the rotating planet, undergoes small disturbances, an important class of wave motions

results. The study of such a system originated with Laplace in the early nineteenth century, and has led to many insights into atmospheric behavior; in particular it underlies the theory of tides (Section 4.3) and global normal modes (Section 4.4).

We start with the linearized equations [Eqs. (3.4.2)], and set the basic flow $\bar{u}$ to zero; thus $\bar{\theta}_\phi$ also vanishes, by Eq. (3.4.1c). Moreover, we use Eq. (3.4.2c) to substitute for $\theta'$ in Eq. (3.4.2e) and use the definition $N^2(z) \equiv H^{-1}R\bar{\theta}_z e^{-\kappa z/H}$ [cf. Eq. (3.2.13)] to replace $\bar{\theta}_z$ in Eq. (3.4.2e). There result

$$u'_t - fv' + (a\cos\phi)^{-1}\Phi'_\lambda = X', \tag{4.2.1a}$$

$$v'_t + fu' + a^{-1}\Phi'_\phi = Y', \tag{4.2.1b}$$

$$(a\cos\phi)^{-1}[u'_\lambda + (v'\cos\phi)_\phi] + \rho_0^{-1}(\rho_0 w')_z = 0, \tag{4.2.1c}$$

$$\Phi'_{zt} + N^2 w' = \kappa J'/H, \tag{4.2.1d}$$

where the diabatic term $\kappa J'/H$ also equals $H^{-1}RQ'e^{-\kappa z/H}$; see Section 3.1.1. If the lower boundary is flat, and located at $z^* = 0$, the linearized version of Eq. (3.1.6a) becomes

$$\Phi'_t + w'\bar{\Phi}_z = 0 \qquad \text{at} \quad z = 0;$$

using Eq. (3.4.1b) and the relation between temperature and potential temperature, this can be written

$$\Phi'_t + \frac{R\bar{T}(0)w'}{H} = 0 \qquad \text{at} \quad z = 0. \tag{4.2.2}$$

The upper boundary condition depends on the problem in hand: see Section 4.3.3.

In this section we consider the conservative or unforced case $X' = Y' = J' = 0$, and use the method of separation of variables to investigate the solutions of Eq. (4.2.1). A first step is to separate the vertical dependence from the horizontal and time dependence; it turns out that the natural way to do this is by setting

$$(u', v', \Phi') = e^{z/2H}U(z)[\tilde{u}(\lambda, \phi, t), \tilde{v}(\lambda, \phi, t), \tilde{\Phi}(\lambda, \phi, t)] \tag{4.2.3a}$$

and

$$w' = e^{z/2H}W(z)\tilde{w}(\lambda, \phi, t). \tag{4.2.3b}$$

Substitution of Eq. (4.2.3a) into Eqs. (4.2.1a,b) (with $X' = Y' = 0$) and cancellation of the $e^{z/2H}U$ factor yields the following two equations, which involve only the $(\lambda, \phi, t)$ dependence:

$$\tilde{u}_t - f\tilde{v} + (a\cos\phi)^{-1}\tilde{\Phi}_\lambda = 0, \tag{4.2.4a}$$

$$\tilde{v}_t + f\tilde{u} + a^{-1}\tilde{\Phi}_\phi = 0, \tag{4.2.4b}$$

while substitution of Eqs. (4.2.3a,b) into Eqs. (4.2.1c,d) (with $J' = 0$) yields the following pair of equations, involving $z$ dependence as well:

$$U(a\cos\phi)^{-1}[\tilde{u}_\lambda + (\tilde{v}\cos\phi)_\phi] + \left(W_z - \frac{W}{2H}\right)\tilde{w} = 0, \qquad (4.2.5a)$$

$$\left(U_z + \frac{U}{2H}\right)\tilde{\Phi}_t + N^2 W\tilde{w} = 0. \qquad (4.2.5b)$$

Examination of the expressions of Eqs. (4.2.3) and the $z$-dependent terms of Eq. (4.2.5a) shows that we can choose

$$U = \frac{dW}{dz} - \frac{W}{2H} \qquad (4.2.6a)$$

without loss of generality. Substitution of Eq. (4.2.6a) into Eq. (4.2.5b) yields

$$-\left(W_{zz} - \frac{W}{4H^2}\right)\Big/ N^2 W = \tilde{w}/\tilde{\Phi}_t = (gh)^{-1} \qquad (4.2.6b)$$

say, where $(gh)^{-1}$ is a separation constant and $h$ has dimensions of length. Then Eqs. (4.2.6a,b) and Eq. (4.2.5a) give

$$(a\cos\phi)^{-1}[\tilde{u}_\lambda + (\tilde{v}\cos\phi)_\phi] + (gh)^{-1}\tilde{\Phi}_t = 0, \qquad (4.2.4c)$$

while the outer terms in Eq. (4.2.6b) yield

$$\frac{d^2W}{dz^2} + \left(\frac{N^2}{gh} - \frac{1}{4H^2}\right)W = 0. \qquad (4.2.7a)$$

The three equations [Eqs. (4.2.4a,b,c)] for the horizontal and time structure are called *Laplace's tidal equations*, and are identical to those for small disturbances to a thin layer of fluid on a sphere, where the fluid has mean depth $h$ much less than the radius $a$ of the sphere, $\tilde{u}$ and $\tilde{v}$ are the velocity components, and $g^{-1}\tilde{\Phi}$ is the departure of the fluid depth from its mean value. The separation constant $h$ is called the *equivalent depth.* Equation (4.2.7a) is called the *vertical structure equation*; from Eqs. (4.2.2), (4.2.3), and (4.2.6), the lower boundary condition can be written

$$\frac{dW}{dz} + \left(\frac{R\bar{T}(0)}{gh} - \frac{1}{2}\right)\frac{W}{H} = 0 \qquad \text{at} \quad z = 0. \qquad (4.2.7b)$$

It should be noted that $h$ is not the vertical scale of $W(z)$. For example, when $N$ is constant and $0 < h < 4N^2H^2/g$, Eq. (4.2.7a) has particular solutions that are sinusoidal in $z$ with vertical wavelength $\lambda_v = 2\pi[(N^2/gh) - 1/4H^2]^{-1/2}$; the variation of $\lambda_v$ with $h$ is shown in Fig. 4.1.

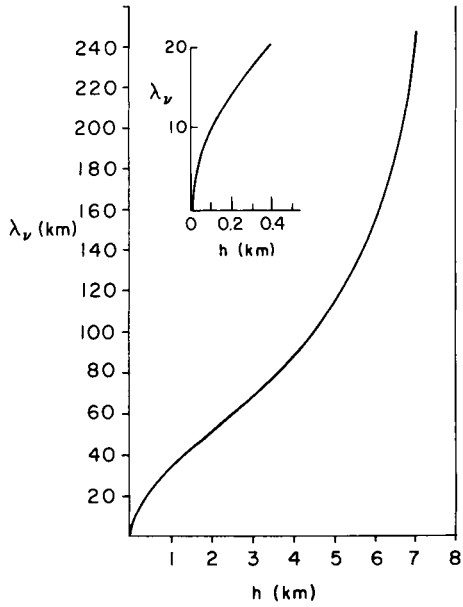


**Fig. 4.1.** The wavelength $\lambda_\nu$ as a function of the equivalent depth $h$ for $0 < h < 4N^2H^2/g$ in an isothermal atmosphere with $\bar{T} = 240$ K. In this case $H = 7$ km and $4N^2H^2/g = 4\kappa H = 8$ km by Eq. (3.2.13) and the definition $H = RT_s/g$, together with $\kappa = 2/7$. The inset gives an expanded view of the region near the origin.

The standard procedure for finding solutions to Laplace's tidal equations [Eqs. (4.2.4)] is to pose the sinusoidal forms

$$\{\tilde{u}, \tilde{v}, \tilde{\Phi}\} = \mathrm{Re}\{[\hat{u}(\phi), \hat{v}(\phi), \hat{\Phi}(\phi)] \exp i(s\lambda - 2\Omega\sigma t)\} \tag{4.2.8}$$

with zonal wavenumber $s$ (an integer) and period $2\pi/2\Omega\sigma$ [or $(2\sigma)^{-1}$ in days]. Solving Eqs. (4.2.4a,b) for $\hat{u}$ and $\hat{v}$ and substituting in Eq. (4.2.4c), we obtain *Laplace's tidal equation*,

$$\mathscr{L}\hat{\Phi} + \gamma\hat{\Phi} = 0. \tag{4.2.9}$$

Here $\gamma \equiv 4\Omega^2a^2/gh$ is called Lamb's parameter and

$$\mathscr{L} \equiv \frac{d}{d\mu}\left[\frac{(1-\mu^2)}{(\sigma^2-\mu^2)}\frac{d}{d\mu}\right] - \frac{1}{\sigma^2-\mu^2}\left[\frac{-s(\sigma^2+\mu^2)}{\sigma(\sigma^2-\mu^2)} + \frac{s^2}{1-\mu^2}\right] \tag{4.2.10}$$

is a second-order ordinary differential operator in the variable

$$\mu \equiv \sin\phi \qquad (-1 \leq \mu \leq 1) \tag{4.2.11}$$

and depends on $s$ and $\sigma$. The appropriate boundary conditions are that $\hat{\Phi}$ is bounded at the poles, $\mu = \pm 1$.

Given these boundary conditions, Eq. (4.2.9) is an eigenvalue problem and can be solved numerically. For example, if $s$ and $\sigma$ are specified, as in the theory of thermally forced tides to be treated in Section 4.3, a set of eigenvalues $\gamma_n^{(\sigma,s)}$ [or equivalent depths $h_n^{(\sigma,s)}$] and corresponding eigenfunctions $\Theta_n^{(\sigma,s)}$ can be found, which are bounded at the poles and satisfy

$$\mathscr{L}\Theta_n^{(\sigma,s)} + \gamma_n^{(\sigma,s)}\Theta_n^{(\sigma,s)} = 0 \tag{4.2.12}$$

for integer values of $n$. The $\Theta_n$ are called *Hough functions* and, together with $\gamma_n$, have been extensively tabulated (e.g., by Longuet-Higgins, 1968). It should be noted that for some choices of $\sigma$, $s$, and $n$, $\gamma_n^{(\sigma,s)}$ and thus the equivalent "depth" $h_n^{(\sigma,s)}$ can be negative; moreover, the frequencies of the modes with $\gamma < 0$ all satisfy

$$|\sigma| < 1. \tag{4.2.13}$$

Some examples of the variation of $|\gamma|^{-1/2}$ with $\sigma$ and $n$ at fixed zonal wave number $s$ are shown in Fig. 4.2, for both positive and negative $\gamma$. The modes of eastward phase speed in Fig. 4.2a can all be regarded as (inertio-) gravity waves, except in the limit $\gamma^{-1/2} \to 0$ (to the left of the diagram), when the lowest two curves represent the Kelvin wave and mixed planetary-gravity (or Rossby-gravity) wave, respectively. The modes of westward phase speed in Fig. 4.2b fall into three classes: the central curve represents the mixed pl-netary-gravity wave, those above it (of higher frequency) represent gravity waves, while those below (of lower frequency) represent planetary waves.

Longuet-Higgins gives a more precise system of classification for these modes, and for those of negative equivalent depth in Figs. 4.2c,d. He also considers the limits of large and small $|\gamma|^{-1/2}$ in detail: for example, as $\gamma^{-1/2} \to \infty$ (i.e., large positive equivalent depths, on the right of the diagrams) the gravity waves, indexed by $n_G$ in that limit, obey the dispersion relation

$$2\Omega\sigma \sim \pm[n_G(n_G+1)gh]^{1/2}a^{-1}, \tag{4.2.14a}$$

(see Section 4.6.1), and the corresponding Hough functions reduce to the associated Legendre polynomials $P_n^s(\mu)$. It can be shown that these limiting modes are divergent but irrotational—that is, $\tilde{\Phi} \not\equiv 0$ but the relative vorticity $(a\cos\phi)^{-1}[\tilde{v}_\lambda - (\tilde{u}\cos\phi)_\phi] \equiv 0$. On the other hand, the planetary waves and mixed mode, indexed by $n_R$, become nondivergent ($\tilde{\Phi} \equiv 0$) but rotational as $\gamma^{-1/2} \to \infty$, with relative vorticity proportional to $P_n^s$ and dispersion relation

$$2\Omega\sigma \sim \frac{-2\Omega s}{n_R(n_R+1)}; \tag{4.2.14b}$$

see the end of Section 4.5.2.

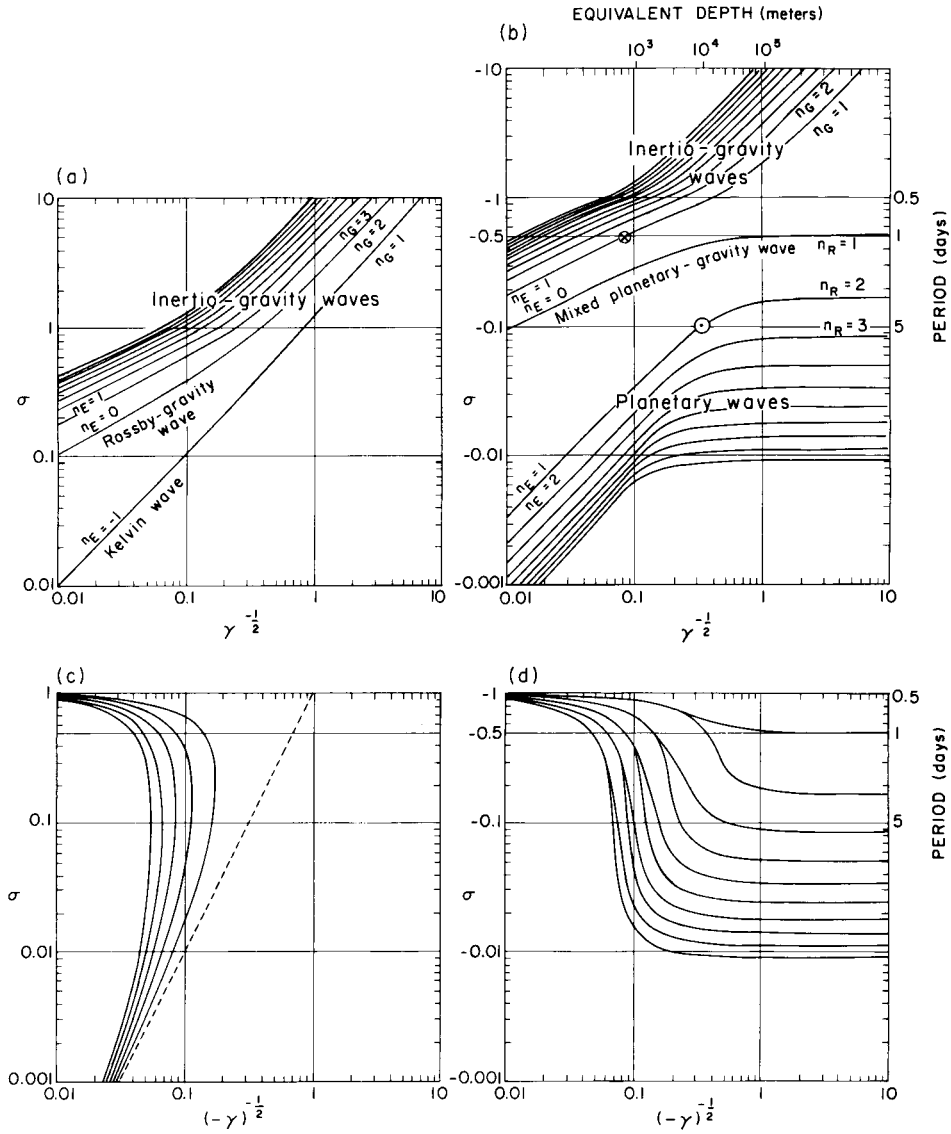


**Fig. 4.2.** Plots of $|\gamma|^{-1/2} \equiv (g|h|)^{1/2}/2\Omega a$ versus frequency $\sigma$ for zonal wave number $s = 1$. Positive equivalent depths ($\gamma > 0$): (a) eastward phase speed ($\sigma > 0$), (b) westward phase speed ($\sigma < 0$). Negative equivalent depths ($\gamma < 0$): (c) eastward phase speed ($\sigma > 0$), (d) westward phase speed ($\sigma < 0$). In (b) and (d) some selected periods in days are given, and a horizontal line is drawn at the diurnal period ($\sigma = -\frac{1}{2}$). In (b) some equivalent depths are given (for $g = 9.8\ \mathrm{m\,s^{-1}}$, $\Omega = 7.3 \times 10^{-5}\ \mathrm{s^{-1}}$, $a = 6.4 \times 10^{6}$ m). The cross in (b) indicates the main propagating diurnal tidal mode (Section 4.3.3), and the circle indicates the "5-day wave" (Section 4.4). The indices $n_G$ and $n_R$ on the right-hand ends of some of the curves appear in Eqs. (4.2.14a,b). The indices $n_E$ on the left-hand ends correspond to the index $n$ used in Section 4.7 for equatorially trapped modes. [Adapted from Longuet-Higgins (1968).]

As $\gamma^{-1/2} \to 0$ (small positive equivalent depths, on the left of the diagrams), all modes become trapped near the equator: these equatorial waves are more readily studied using beta-plane geometry, and will be considered in Section 4.7. Asymptotic forms are also available for $\gamma < 0$; these include polar-trapped modes as $(-\gamma)^{-1/2} \to 0$, and nondivergent planetary waves with dispersion relation Eq. (4.2.14b) as $(-\gamma)^{-1/2} \to \infty$.

A different approach is used in the theory of free global normal modes, to be discussed in Section 4.4. Here $h$ is sought as an eigenvalue of the vertical structure equation [Eq. (4.2.7a)], subject to the lower boundary condition of Eq. (4.2.7b) and an appropriate upper boundary condition. The corresponding $\gamma \equiv 4\Omega^2 a^2/gh$, together with the zonal wave number $s$, is substituted into Laplace's tidal equation [Eq. (4.2.9)], which is now solved as an eigenvalue problem for $\sigma$, giving a set of eigenfrequencies (which can be read off from diagrams such as Figs. 4.2a,b) and corresponding Hough functions.

## 4.3 Atmospheric Thermal Tides

Atmospheric tides are global-scale daily oscillations, which are primarily forced by diurnal variations of the heating due to absorption of solar ultraviolet radiation by atmospheric water vapor and ozone. The solar and lunar gravitational forcing that produces ocean tides is much less important for the atmosphere, and we shall concentrate on thermally driven tides here. We shall further restrict attention to *migrating* tides, which move with the sun. Nonmigrating tides are associated, for example, with topography and geographically fixed tropospheric heat sources; they have received comparatively little theoretical attention. Migrating tides, on the other hand, have been studied extensively; they can sometimes propagate through great depths of the atmosphere, and can attain large amplitudes at some heights, especially in the thermosphere. Even in the mesosphere tidal temperature amplitudes can easily exceed 10 K, and can for example lead to problems in the interpretation of satellite data sampled once per day.

### *4.3.1 Summary of the Main Results of Atmospheric Tidal Theory*

The basic ideas of tidal theory are quite simple, although some of the mathematical details are a little complicated. Thus, before going into the analysis in depth, we shall summarize the main results.

The first point to notice is that the solar heating is only active during the day, with a time variation which might look something like that shown in Fig. 4.3 at a point in midlatitudes. A Fourier analysis of this curve will

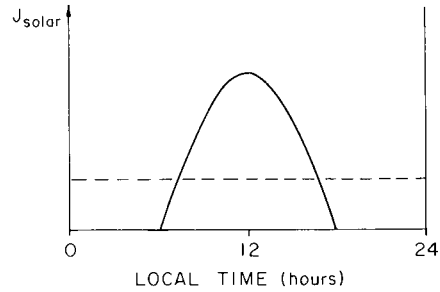


**Fig. 4.3.** Schematic diagram of the typical daily variation of the solar heating $J_{solar}$ (heavy curve) at a point in midlatitudes. The horizontal dashed line represents the diurnal or zonal average of $J_{solar}$, which is assumed to be balanced by a zonal-mean infrared cooling, so that the net $\bar{J} = 0$. The term $J'$ is represented by the departure of the heavy curve from the dashed curve.

include a steady component, a diurnal component (with a 24-hr period), a somewhat smaller semidiurnal component (with a 12-hr period), and so on. The response of the atmosphere to this heating can likewise be decomposed into a steady part, and diurnal, semidiurnal and higher-frequency oscillations. An old puzzle, raised by Kelvin in 1882, was to explain why the *semidiurnal* surface pressure oscillation (about 1 mb in amplitude) is larger and more regular than the *diurnal*. The answer is best explained by describing the response of the whole middle and lower atmosphere to the diurnal and semidiurnal heating, as currently understood from theory and observation.

It transpires that the forced *semidiurnal* tidal oscillation has a large vertical wavelength (greater than 100 km). This allows it to be excited rather efficiently by the deep ozone heating region, which is present around the stratopause. Moreover it can easily propagate to the ground and hence show up in surface pressure fluctuations. It is regular because the ozone heating is regular, and its latitudinal structure is fairly uniform.

The *diurnal* tide, on the other hand, has a more complex behavior. Between 30°N and 30°S it can propagate vertically, with a wavelength of about 28 km. Polewards of 30°, however, it is trapped in the vertical, close to its forcing region. As a result, the vertically propagating modes forced by the deep ozone heating tend to interfere destructively, and thus have small amplitude at the ground, while the trapped modes forced by the ozone never reach the ground at all. However, the comparatively shallow water-vapor heating region in the troposphere can excite this tide quite effectively, although this heating is somewhat intermittent in space and time. The resulting surface pressure oscillation is also intermittent. On the other hand, at the stratopause and above, the diurnal oscillation can be as strong as the semidiurnal.

### *4.3.2 Observations of Tides in the Middle Atmosphere*

The surface pressure record is by far the largest existing atmospheric tidal data set, and it was the predominance of the semidiurnal component in this record that prompted Kelvin's question of 1882 and some of the earlier theories of atmospheric tides; data on other tropospheric tidal parameters, such as surface temperature and wind, are also very extensive now. Observations of tides in the middle atmosphere, on the other hand, are sparser, although a number of measurement techniques are currently available; these techniques will be briefly discussed here.

In the lower stratosphere, up to about 30 km altitude, wind observations from the tracking of meteorological balloons have provided data for large areas of the world and over many years. These data have been analyzed to provide estimates of the diurnal and semidiurnal tides, and show considerable vertical and horizontal structure and the presence of both migrating and nonmigrating components: see Fig. 4.4.

Above 30 km, a number of measurement techniques based on rockets and radars can be used. Rocket observations are mainly confined to altitudes below about 60 km, although there are a few important observations between 60 and 100 km. The radar techniques (summarized in Section 1.5) primarily provide wind measurements in the altitude range 70–110 km. The rocket and radar data have provided amplitudes and vertical wavelengths of both the diurnal and semidiurnal tides above selected locations on the globe and for selected periods of time: see Figs. 4.5 and 4.6.

These rocket and radar observations are necessarily restricted in geographical, and sometimes temporal, coverage, and this can be a drawback when comparison with theoretical calculations of global tidal structures is attempted. A recent advance has been the employment of simultaneous measurements from two Stratospheric Sounding Units on different NOAA satellites to obtain near-global tidal observations over long periods of time at several levels in the upper stratosphere. Although these observations have limited vertical resolution, satellite techniques of this kind promise a great expansion of the observational basis of our knowledge of tides in the middle atmosphere, thus providing a more critical test of theory. Such comparisons between theory and observations as are available at present are mentioned briefly in Section 4.3.4.

### *4.3.3 Classical Tidal Theory*

We shall now outline the "classical" theory of tides, as given for example by Chapman and Lindzen (1970), who consider linear disturbances to an

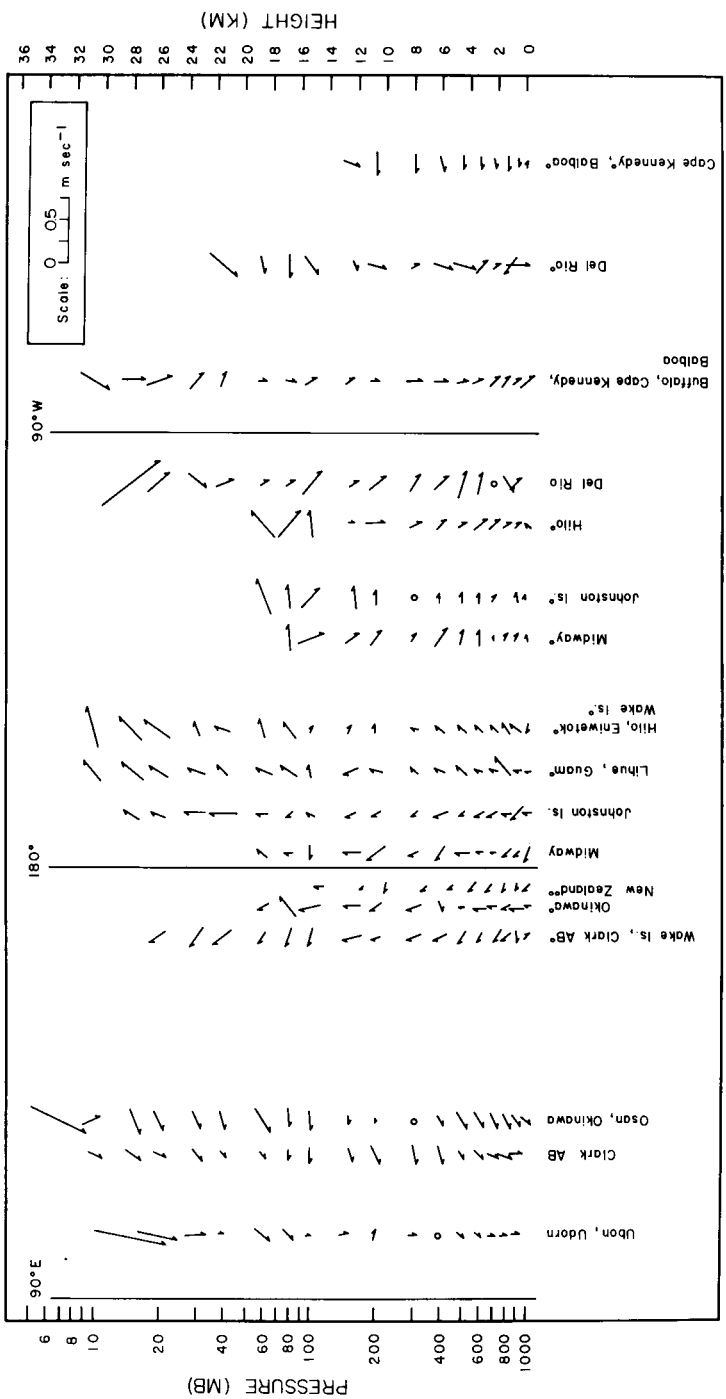


**Fig. 4.4.** Longitude–height or time–height section for the semidiurnal wind component for June–July, based on several years of radiosonde data. Arrows are centered on the longitude of the stations or the mean longitudes of groups of stations, and their directions indicate the flow direction, with upward corresponding to poleward. Note the roughly uniform rotation of the wind vectors with longitude and time, the increase in amplitude with height, and the lack of phase variation with height. [After Wallace and Tadd (1974).]

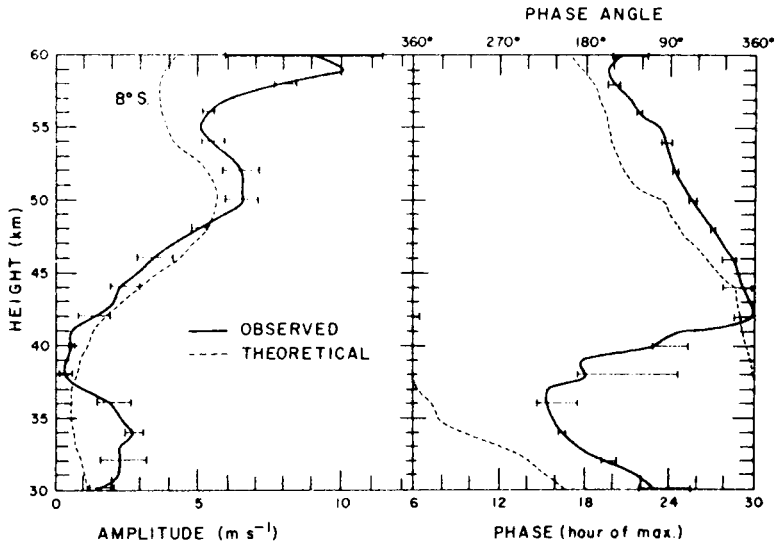


**Fig. 4.5.** Vertical variation of the amplitude and phase of the diurnal northerly wind component, as determined from rockets launched at Ascension Island (8°S). Also shown are theoretical calculations by Lindzen (1967), based on classical tidal theory (see Section 4.3.3). [After Reed *et al.* (1969). American Meteorological Society.]

atmosphere that is basically at rest. The set of Eqs. (4.2.1) is therefore used, together with suitable boundary conditions and a specified thermal forcing term $\kappa J'/H$ on the right of Eq. (4.2.1d); the mechanical forcing or dissipation terms $X'$ and $Y'$ are set to zero. The restriction to migrating tides means that all variables are taken to depend only on local time, latitude, and height; thus, for example, $J' = J'(\lambda + \Omega t, \phi, z)$, since $t + \lambda/\Omega$ is the local time at longitude $\lambda$ if $t$ is Greenwich Mean Time. (In accordance with the notation of Section 3.3, $J'$ denotes the deviation of $J$ from the zonal mean net heating $\bar{J}$. As seen from Fig. 4.3, the zonal-mean solar heating is nonzero; however, it will be assumed to be balanced by a zonal-mean infrared cooling, so that $\bar{J} = 0$.)

Since $J'$ is periodic, it can be expanded in Fourier harmonics: thus

$$J' = \mathrm{Re} \sum_{s=1}^{\infty} J^{(s)}(\phi, z) e^{is(\lambda + \Omega t)} \tag{4.3.1}$$

where the coefficients $J^{(s)}$ are assumed known from a radiative-photochemical calculation. (This may not be a very accurate assumption: for example, the ozone distribution, which partly determines the heating, will depend to some extent on the tidal response to the heating.) The $s = 1$ component is the *diurnal* heating, and corresponds to $\sigma = -\frac{1}{2}$ in the notation

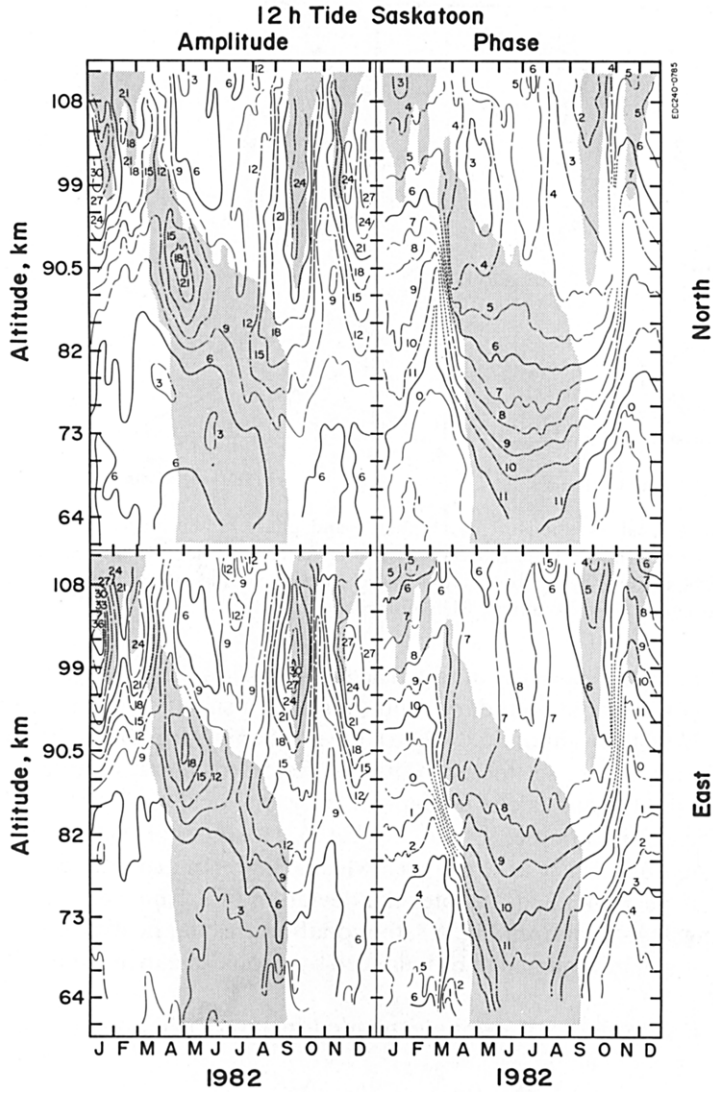


**Fig. 4.6.** Amplitude ($m\,s^{-1}$) and phase (local time of maximum) of the semidiurnal tidal wind components in the upper mesosphere and lower thermosphere, as measured by a partial reflection radar technique at Saskatoon (52°N) during 1982. The shaded region indicates that the time-mean zonal wind is easterly, the unshaded region that it is westerly. [After Manson and Meek (1986).]

of Eq. (4.2.8); the $s = 2$ component is the *semidiurnal* heating and corresponds to $\sigma = -1$; higher terms are seldom considered.

The next step is to expand each $J^{(s)}(\phi, z)$ in the Hough functions introduced in Section 4.2. (This procedure is analogous to that adopted in the theory, say, of the forced vibration of a stretched string, in which the forcing is expanded in terms of the eigenmodes of the unforced string.) In particular, $J^{(1)}$ is expanded in diurnal Hough functions $\Theta_n^{(-1/2,1)}$ which we shall call $\Theta_n^{(1)}$ for short, while $J^{(2)}$ is expanded in semidiurnal Hough functions $\Theta_n^{(-1,2)} \equiv \Theta_n^{(2)}$. Since modes of negative equivalent depth exist in the diurnal case ($\sigma = -\frac{1}{2}$), these must be included in the expansion of $J^{(1)}$. However, Eq. (4.2.13) shows that such modes are absent for semidiurnal and higher frequencies. Figures 4.2b,d for $s = 1$ include horizontal lines at the diurnal frequency, whose intersections with the plotted curves indicate the relevant modes and their equivalent depths. For positive equivalent depths (Fig. 4.2b) the relevant Hough functions all represent gravity modes, in the sense of Section 4.2, except for the gravest diurnal mode, which is of mixed type, has an infinite equivalent depth ($\gamma^{-1/2} \to \infty$), and is antisymmetric about the equator.

As an example, we shall consider the diurnal forcing $J^{(1)}(\phi, z)e^{i(\lambda+\Omega t)}$ and the atmospheric response to it. We write

$$J^{(1)}(\phi, z) = \sum_n J_n^{(1)}(z)\Theta_n^{(1)}(\mu) \tag{4.3.2}$$

where $\mu = \sin\phi$ as before; thus $J_n^{(1)}$ is the projection of the diurnal heating onto the $n$th diurnal Hough function. We look for a response with a similar migrating form, say, $w^{(1)}(\phi, z)e^{i(\lambda+\Omega t)}$ for the vertical velocity, where

$$w^{(1)}(\phi, z) = \sum_n e^{z/2H} W_n^{(1)}(z)\Theta_n^{(1)}(\mu), \tag{4.3.3}$$

by analogy with Eqs. (4.3.2) and (4.2.3b) (and with the vibrating string example, where the response to the forcing is also expanded in eigenmodes). We return to Eqs. (4.2.1), set $X' = Y' = 0$, and give all primed variables the diurnal $e^{i(\lambda+\Omega t)}$ dependence. The diurnal velocity amplitudes $u^{(1)}$ and $v^{(1)}$ can be expressed in terms of $\Phi^{(1)}$, using Eqs. (4.2.1a,b), and then expressed in terms of $w^{(1)}$ and $J^{(1)}$ by means of Eq. (4.2.1d). On substitution into Eq. (4.2.1c) we obtain a complicated partial differential equation in $z$ and $\mu$ for $w^{(1)}$ in terms of $J^{(1)}$; however, on using Eqs. (4.3.2) and (4.3.3), and Laplace's tidal equation [Eq. (4.2.12)] for $\Theta_n^{(1)}$, the $\mu$ dependence separates out, leaving the inhomogeneous vertical structure equation [cf. Eq. (4.2.7a)]

$$\frac{d^2W_n^{(1)}}{dz^2} + \left[\frac{N^2}{gh_n^{(1)}} - \frac{1}{4H^2}\right] W_n^{(1)} = \frac{\kappa J_n^{(1)}(z)e^{-z/2H}}{gHh_n^{(1)}}, \tag{4.3.4}$$

with homogeneous lower boundary condition [cf. Eq. (4.2.7b)]

$$\frac{dW_n^{(1)}}{dz} + \left[\frac{R\bar{T}(0)}{gh_n^{(1)}} - \frac{1}{2}\right]\frac{W_n^{(1)}}{H} = 0 \qquad \text{at} \quad z = 0, \tag{4.3.5}$$

where $h_n^{(1)}$ is the $n$th diurnal equivalent depth.

The upper boundary condition needs careful consideration, and we follow the approach outlined in Section 3.1.2.b. We suppose that above some height $z_2$ the forcing $J_n^{(1)}$ vanishes and the mean temperature $\bar{T}(z)$ becomes constant, $T_\infty$ say, so that $N^2 = R\kappa T_\infty/H^2 = g\kappa T_\infty/HT_s \equiv N_\infty^2 =$ constant there. Thus for $z > z_2$, Eq. (4.3.4) becomes

$$\frac{d^2W_n^{(1)}}{dz^2} + \left[\frac{N_\infty^2}{gh_n^{(1)}} - \frac{1}{4H^2}\right]W_n^{(1)} = 0,$$

with solutions that are exponential or sinusoidal in $z$ according as the expression in square brackets is negative or positive. If it is negative, that is, if $h_n^{(1)} < 0$ or $h_n^{(1)} > 4H^2N_\infty^2/g = 4\kappa HT_\infty/T_s$, then the decaying solution, with $W_n$ proportional to

$$\exp -\left[\frac{1}{4H^2} - \frac{N_\infty^2}{gh_n^{(1)}}\right]^{1/2} z,$$

is clearly the one to be selected, and this provides the required upper boundary condition. Using Eqs. (4.2.3a), (4.2.6a), and (4.2.7a) and the fact that $\rho_0 \propto e^{-z/H}$, it can be shown that the mean wave energy per unit volume, $\frac{1}{2}\rho_0(\overline{u'^2} + \overline{v'^2} + \overline{\Phi_z'^2}/N^2)$ [see Eq. (3.6.3)], decays with height for this solution. However, if $0 < h_n^{(1)} < 4H^2N_\infty^2/g$, then propagating solutions exist, with $W_n^{(1)} \propto e^{imz}$ for $z > z_2$ where

$$m = \pm\left[\frac{N_\infty^2}{gh_n^{(1)}} - \frac{1}{4H^2}\right]^{1/2} \tag{4.3.6}$$

is the vertical wave number. The wave energy per unit volume is independent of $z$ for either sign of $m$, and the appropriate choice has to be made by computing the vertical component of the group velocity, $c_g^{(z)}$, and demanding that it be positive. This is the "radiation condition," which states that information must be traveling upward, and not downward, at great heights: see Section 3.1.2. We have $c_g^{(z)} \equiv \partial\omega/\partial m$, where $\omega = 2\Omega\sigma$ is the frequency. Thus

$$\begin{aligned} c_g^{(z)} &\equiv \frac{\partial\omega}{\partial m} = 2\Omega\frac{\partial\sigma}{\partial m} = 4\Omega m\frac{\partial\sigma}{\partial m^2} \\ &= 4\Omega m\left(\frac{\partial\sigma}{\partial h}\right)\Big/\left(\frac{\partial m^2}{\partial h}\right) = -4\Omega m\left(\frac{\partial\sigma}{\partial h}\right)\Big/\left(\frac{N_\infty^2}{gh^2}\right) \end{aligned} \tag{4.3.7}$$

by Eq. (4.3.6), where indices on $h$ have been dropped for clarity. Referring to Fig. 4.2b, we see that for all the relevant modes of finite, positive $h$ (which

are in fact gravity waves), $\partial(-\sigma)/\partial h > 0$, so that $c_g^{(z)}$ has the same sign as $m$, by Eq. (4.3.7). To satisfy the radiation condition, the positive sign must be chosen in Eq. (4.3.6), thus giving the upper boundary condition in the propagating-wave case.

The numerical solution of the vertical structure equation [Eq. (4.3.4)] for $W_n^{(1)}(z)$, subject to the appropriate boundary conditions, is straightforward. The series of Eq. (4.3.3) is then summed to obtain $w^{(1)}(\phi, z)$, and $u^{(1)}$, $v^{(1)}$, and $\Phi^{(1)}$ can be found from Eq. (4.2.1); a precisely similar procedure can be used for the semidiurnal response $w^{(2)}$, etc. Full details are given by Chapman and Lindzen (1970).

Although the global forms of the tidal structure are quite complicated, some general features can be deduced from basic properties of the vertical structure equation and Laplace's tidal equation. First note from Eq. (4.3.4) that if $0 < h < 4N^2H^2/g$ a tidal mode is roughly sinusoidal in the vertical, with wavelength given locally by

$$\lambda_v = 2\pi\left[\frac{N^2(z)}{gh} - \frac{1}{4H^2}\right]^{-1/2}$$

(The modal index $n$ has again been omitted.) In the *diurnal* case some modes have $h < 0$, and the mixed mode of Fig. 4.2b has $h = \infty$; these modes are trapped in the vertical near to the forcing region. However, the diurnal gravity waves all propagate: the leading symmetric one, marked with a cross in Fig. 4.2b, has $h \approx 690$ m and $\lambda_v \approx 28$ km. Investigation of the horizontal Hough function structure (see Longuet-Higgins, 1968 and Chapman and Lindzen, 1970) shows that the propagating modes are confined equatorward of 30° latitude. (This is the latitude at which $|f| = 2\Omega|\sigma|$ or $|\mu| = |\sigma|$ for the diurnal frequency $\sigma = -\frac{1}{2}$, where Laplace's tidal equation [Eq. (4.2.9)] has apparent singularities: see also Section 4.6.3.) The mixed mode is global in extent with $\Theta \propto \sin\phi\cos\phi$, and the modes of negative equivalent depth are trapped poleward of 30°. Some calculations of the total diurnal response are given in Fig. 4.7; note the strong latitudinal variation, the fact that the amplitude of $T^{(1)}$ is several kelvins in the mesosphere, the vertical wavelength of about 28 km near the equator, and the weak phase variation at high latitudes.

The equivalent depths for the *semidiurnal* tide are all positive, all modes are of the gravity-wave class, and the dominant mode has $h \approx 7.85$ km. For this value, $N^2/gh \approx 1/4H^2$, implying a very large vertical wavelength $\lambda_v$, as mentioned above (see also Fig. 4.1), the vertical structure equation [Eq. (4.3.4)] is replaced by an equation of the form

$$\frac{d^2W}{dz^2} \approx F(z) \equiv \kappa J_1^{(2)}(z)e^{-z/2H}/gHh_1^{(2)} \tag{4.3.8}$$

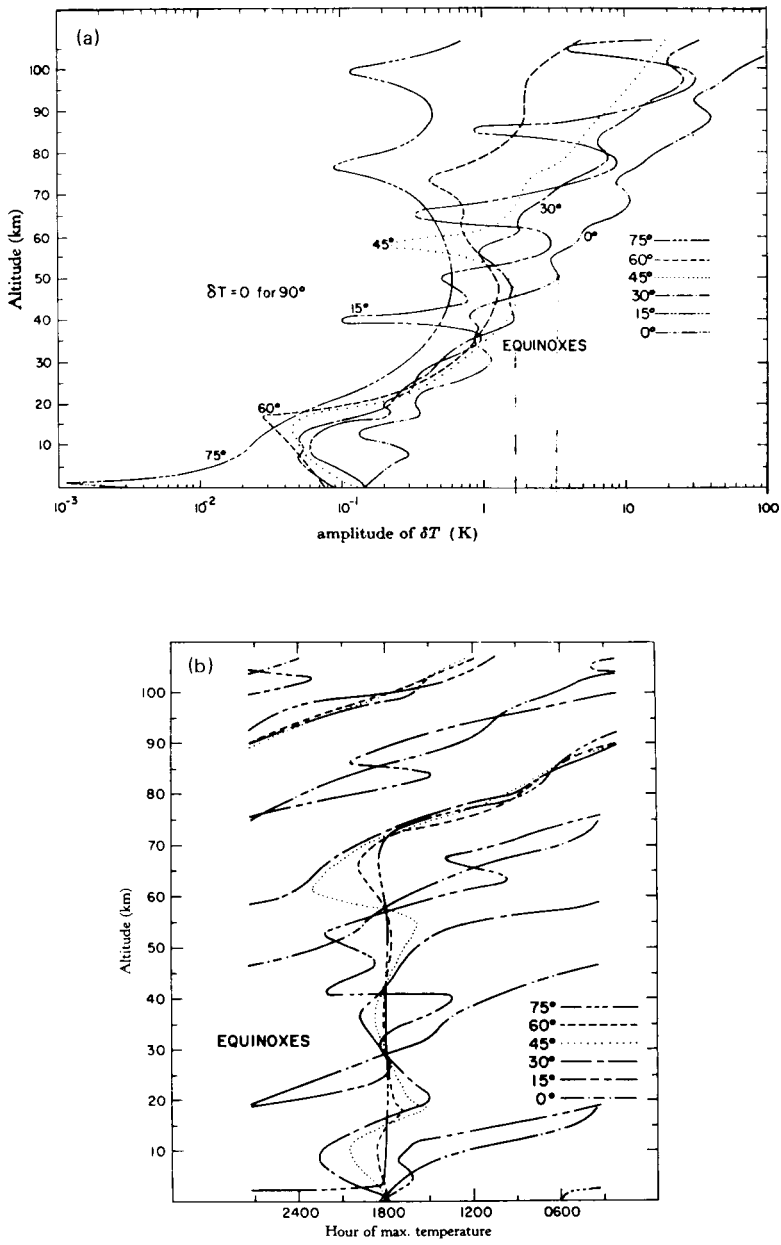


**Fig. 4.7.** (a) Amplitude and (b) phase of solar diurnal component of $T'$ at various latitudes for equinox. [After Lindzen (1967).]

and the lower boundary condition [Eq. (4.3.5)] can be approximated by

$$\frac{dW}{dz} + \frac{W}{2H} \approx 0, \tag{4.3.9}$$

since $RT(0)/gh_1^{(2)} \approx 1$. If the semidiurnal excitation were all concentrated at one level, $z_e$ say, we would have $F(z) = F_e\,\delta(z - z_e)$ and the solution to Eqs. (4.3.8) and (4.3.9) bounded at great heights would take the form $W = (2H - z)F_e$ for $z < z_e$, that is, *below* the excitation level. The corresponding solution for $U$ would be

$$U = -(2 - z/2H)F_e \qquad \text{for} \quad z < z_e$$

by Eq. (4.2.6a), implying that $U$ would change sign at $z = 4H \approx 28$ km if the excitation level $z_e$ were above this height; thus the semidiurnal phases of $u'$ and $v'$ would shift by $\pi$ at $z \approx 4H$, by Eq. (4.2.3a). Detailed calculations show that a similar behavior occurs in the more accurate theory when several semidiurnal Hough modes are included, when $F(z)$ is distributed in the vertical but confined mostly to altitudes above 28 km, and when Eqs. (4.3.4) and (4.3.5) are used rather than Eqs. (4.3.8) and (4.3.9). Some results are given in Fig. 4.8; they show a phase shift in the southward wind at about 28 km altitude, and quite large temperature amplitudes in the mesosphere. They also demonstrate the dominance of ozone in forcing this tide.

### *4.3.4 More Detailed Theory*

In the last decade or so, various improvements on the "classical" theory have been made. Mean winds $\bar{u}(\phi, z)$ and latitudinally varying mean temperatures $\bar{T}(\phi, z)$, for equinox and solstice conditions, have been included, as have Newtonian cooling and (in the thermosphere) molecular viscosity, thermal conductivity, and ion drag. Better parameterizations of ozone and water-vapor heating have been used, and the effects of heating by molecular oxygen included. Such calculations have been performed for height ranges from the ground up to several hundred kilometers.

The theory as it stands now generally agrees fairly well with observations, although, as mentioned in Section 4.3.2, the latter are fairly scanty in the stratosphere and mesosphere. The main discrepancies are between the calculated and observed semidiurnal tides; theory predicts a phase shift in the horizontal winds of 180° at about 28 km altitude (see Fig. 4.8) which is not observed, and the calculated surface pressure phase is 30–60 min later than observed. Recent studies suggest that these differences may be due to the omission of a semidiurnal contribution from latent heating in the tropics. There is also a discrepancy between calculated and observed diurnal tides

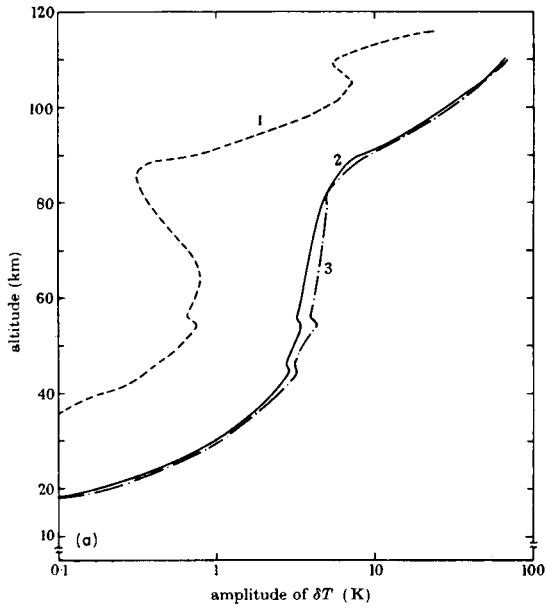


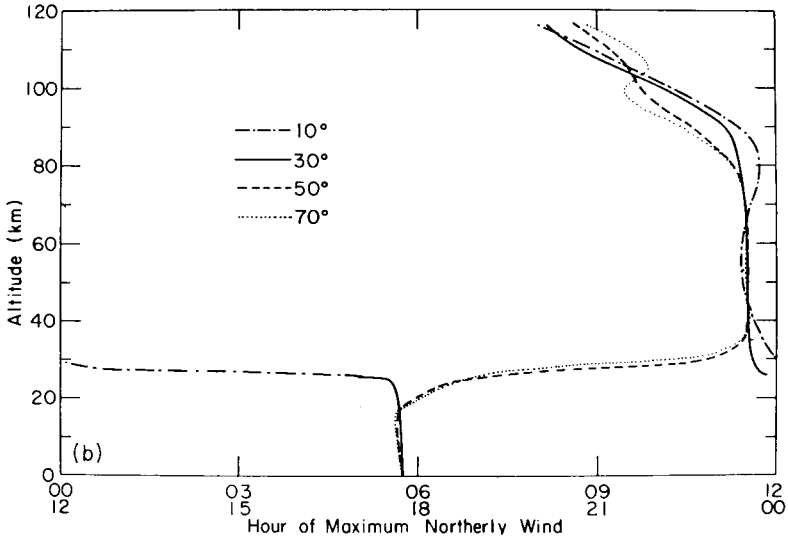


**Fig. 4.8.** (a) Amplitude of semidiurnal component of $T'$ as forced by (1) $H_2O$ only, (2) $H_2O$ and $O_3$, (3) $O_3$ only (Lindzen 1968), and (b) phase of semidiurnal component of $(-v')$ at various latitudes. [After Chapman and Lindzen (1970).]

in the high latitude mesosphere; the observations show a strong seasonal variation in wavelength and phase that is not predicted by theory. As yet, the satellite measurements mentioned in Section 4.3.2 have only been compared with radiance calculations based on classical tidal theory; fair qualitative agreement is found, but some quantitative discrepancies appear, and the reasons for these are at present unresolved.

Another recent development has been the study of nonlinear processes associated with tides: possible implications of such processes for the mean circulation of the middle atmosphere are mentioned briefly in Section 7.3.

## 4.4 Free Traveling Planetary Waves

A well-documented group of atmospheric waves is a class of zonally traveling structures of global scale, which have periods of a few days. Such waves are thought to be examples of free traveling planetary (Rossby) waves or global normal modes and, unlike the thermally driven tides described in the previous section, they are apparently not maintained by traveling forcing effects. They appear for example in surface pressure data, in standard analyses of upper tropospheric radiosonde data, and in satellite data from the stratosphere. Space and time filtering can help to distinguish them from other atmospheric phenomena.

The most prominent mode of this class is the *5-day wave*, a westward-traveling disturbance whose period is close to 5 days and that is approximately sinusoidal in the east–west direction with zonal wave number $s = 1$. The geopotential disturbance $\Phi'$ or temperature disturbance $T'$ associated with this wave is symmetric about the equator, and peaks in midlatitudes. Examples of middle atmosphere observations are presented in Figs. 4.9 and 4.10. The wave has little phase tilt in the vertical, and the observed temperature disturbance grows with height. At the ground the observed pressure fluctuation is about 0.5 mb; in the upper stratosphere at about 40 km altitude ($\approx$2 mb) the temperature fluctuation is approximately 0.5 K. Numerous other traveling modes of this type have also been observed, including a wave-number 1, 16-day wave and a wave-number 3, 2-day wave (Fig. 4.11). More details are given in Section 5.4.

The simplest theory of free modes of this type involves unforced, global-scale, linearized disturbances to an atmosphere that is basically at rest. Equations (4.2.1) are used, with $X' = Y' = J' = 0$; then solutions are sought in the form

$$w' = e^{z/2H}\,\mathrm{Re}[\,W(z)\hat{w}(\phi)\exp i(s\lambda - 2\Omega\sigma t)], \tag{4.4.1}$$

for example [cf. Eqs. (4.2.3b) and (4.2.8)], where $s$ is specified and $\sigma$ is to

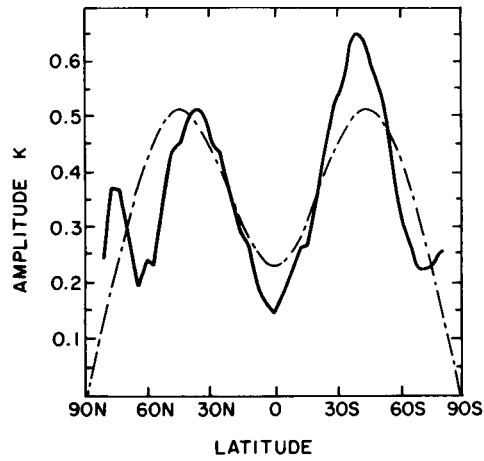


**Fig. 4.9.** Solid curve: brightness temperature amplitude of the 5-day wave as a function of latitude at about 42 km altitude for November 1973, as measured by the Selective Chopper Radiometer on the *Nimbus* 5 satellite. [After Rodgers (1976).] Broken curve: latitudinal structure of the Hough function corresponding to the 5-day wave ($s = 1$, $\sigma \approx -0.1$, $h \approx 10^4$ m). (Courtesy of P. J. Valdes.)

be determined. The method for calculating $\sigma$ proceeds in two stages: first the vertical structure equation [Eq. (4.2.7a)] is solved as an eigenvalue problem for the equivalent depth $h$, subject to the lower boundary condition [Eq. (4.2.7b)] and the requirement that $W \to 0$ (and hence the wave energy per unit volume tends to zero) as $z \to \infty$. [Note that the radiation condition of Section 4.3 is not needed here, since the required modes must be evanescent at great heights. If they were to propagate upward at great heights, a continual forcing mechanism would be needed to maintain their amplitudes at low levels. Thus an eigenvalue $h$ must be such that $N^2/gh < (1/4H^2)$ above some altitude $z_1$, say.]

The second stage of the calculation of $\sigma$ takes the value or values of $h$ found in this way, substitutes them into Laplace's tidal equation for the horizontal structure,

$$\mathscr{L}\hat{w} + (4\Omega^2 a^2/gh)\hat{w} = 0 \tag{4.4.2}$$

[cf. Eq. (4.2.9)], and solves the latter as an eigenvalue equation for $\sigma$. [Recall that $\mathscr{L}$ depends on $s$ and $\sigma$: see Eq. (4.2.10).] The eigenfunctions $\hat{w}$ are given by Hough functions. (Note how this procedure differs from that used in Section 4.3: see also the end of Section 4.2.)

As a simple example, consider an isothermal basic atmosphere, with $\bar{T} = T_s$ = constant; then $N^2 = R\kappa T_s H^{-2} = g\kappa H^{-1}$ by Eq. (3.2.13) and the definition $H = RT_s/g$. In this case a solution $W(z)$ of Eq. (4.2.7a) can only

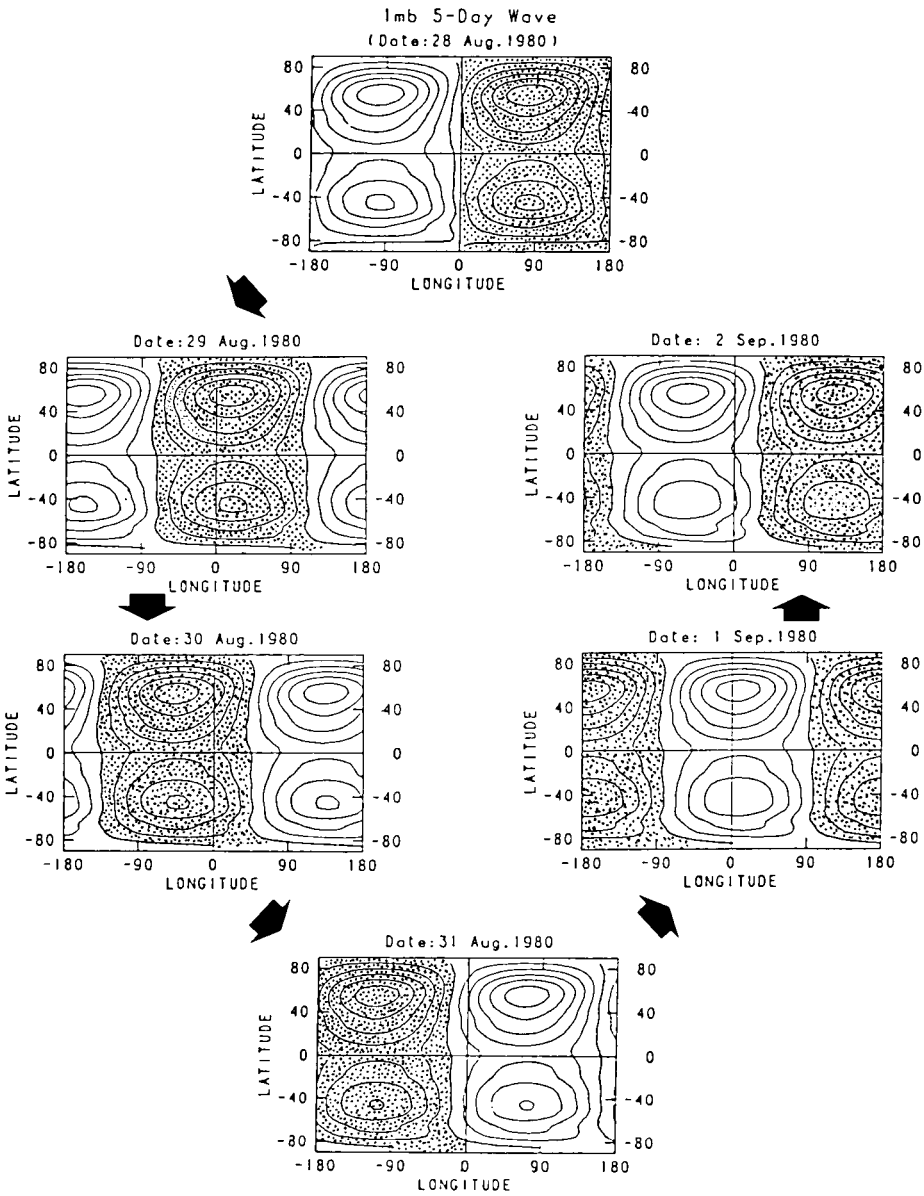


**Fig. 4.10.** The 5-day wave at 1 mb as observed by the Stratospheric Sounding Unit on the *TIROS-N* satellite, for 6 successive days in August–September 1980. The wave-number 1 Fourier component of the geopotential height anomaly has been bandpass-filtered to select periods of 5–6 days (eastward and westward). Note the clear westward-traveling pattern except south of 50°S. Shaded regions denote negative anomalies; the contour interval is 20 m. [After Hirota and Hirooka (1984). American Meteorological Society.]

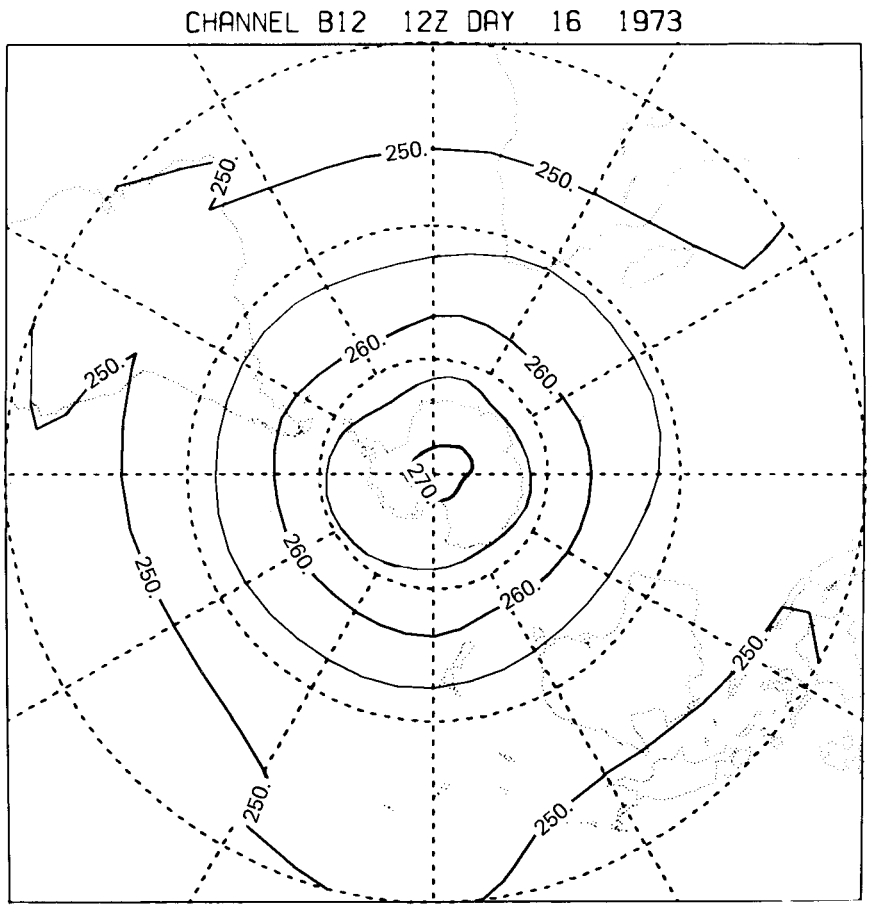


**Fig. 4.11.** The 2-day wave (zonal wave number 3) as observed by the Selective Chopper Radiometer on the *Nimbus* 5 satellite: brightness temperature contours at about 42 km altitude on January 16, 1973. [After Rodgers and Prata (1981).]

satisfy the lower boundary condition of Eq. (4.2.7b) and the upper boundary condition $W \to 0$ as $z \to \infty$ if

$$h = (1 - \kappa)^{-1} H,$$

where $(1 - \kappa)^{-1} = c_p / c_v \approx \frac{7}{5}$, and $c_v$ is the specific heat at constant volume. Then $W(z) \propto \exp[(\kappa - \frac{1}{2})z/H]$ and hence

$$w' \propto e^{\kappa z/H} \tag{4.4.3}$$

by Eq. (4.4.1). Using Eqs. (4.2.6) and (3.1.3c′) it can be shown that $\Phi'$, $u'$, $v'$, and $T'$ have a similar $z$ dependence. The wave thus has no phase tilt in the

vertical, and although the velocity and temperature fields grow with height, the corresponding energy density $\frac{1}{2}\rho_0(\overline{u'^2} + \overline{v'^2} + \overline{\Phi_z'^2}N^{-2})$ [cf. Eq. (3.6.3)] decays with height since $\rho_0 \propto e^{-z/H}$. This is an example of an "external" or "edge" wave, being trapped against the lower boundary. It can be verified that the geometric vertical velocity $Dz^*/Dt$, as opposed to the "log-pressure" velocity $w \equiv Dz/Dt$, vanishes everywhere. Such a vertical structure is also exhibited by an acoustic wave known as the Lamb wave. [Incidentally, no such wave exists in a model with either of the artificial lower boundary conditions $\Phi' = 0$ or $w' = 0$ at $z = 0$: cf. Eqs. (3.1.6b,c).]

The planetary-wave dynamics of this wave enter through the horizontal structure equation [Eq. (4.4.2)]. Taking $T_s = 240$ K, so that $H = 7$ km, we obtain $h \approx 10$ km, and on consulting Fig. 4.2b for $s = 1$ we find that the gravest symmetric westward-traveling planetary mode with this equivalent depth (indicated by a circle) has a period of about 5 days. The corresponding latitudinal structure of $\hat{w}$ (and $\Phi'$) is given in Fig. 4.9. This theoretical solution is close in period and in horizontal and vertical structure to the observed 5-day wave.

This simple type of theory can be extended in several ways. Allowance for a nonisothermal basic temperature $\bar{T}(z)$ does not appear to permit vertical structures significantly different from the external mode form [Eq. (4.4.3)], except possibly for a "ducted" mode peaking near the stratopause. However, the latter is highly susceptible to dissipative processes and is therefore unlikely to have any analogue in the real atmosphere. Inclusion also of horizontally varying mean winds $\bar{u}(\phi)$ still gives a mathematically separable problem, with a modified horizontal structure equation, which can be solved numerically. If the mean wind $\bar{u}$, and thus the mean temperature $\bar{T}$, depends on latitude and height, the problem is no longer separable in $\phi$ and $z$, but numerical methods are still available for solving the linear equations of Eqs. (3.4.2), assuming all disturbance variables to have the $\exp i(s\lambda - 2\Omega\sigma t)$ form of Eq. (4.4.1) and given appropriate boundary conditions. Such a method has been used for example to show that the "5-day" wave period is relatively insensitive to the background wind structure and thus to partially explain why it is such a ubiquitous feature of observations. Details of this approach and further applications to models of the 16-day wave and the 2-day wave are given in Section 5.4.

Observations have suggested the existence of many other global free traveling waves of various periods. Not all of these modes may be even approximately sinusoidal in the zonal direction. For example, a sequence of synoptic maps (Fig. 4.12) shows that a feature that has been identified as a "4-day wave" by Fourier analysis of time series is in reality a localized warm pool that circles the Southern Hemisphere stratosphere in about 4 days.

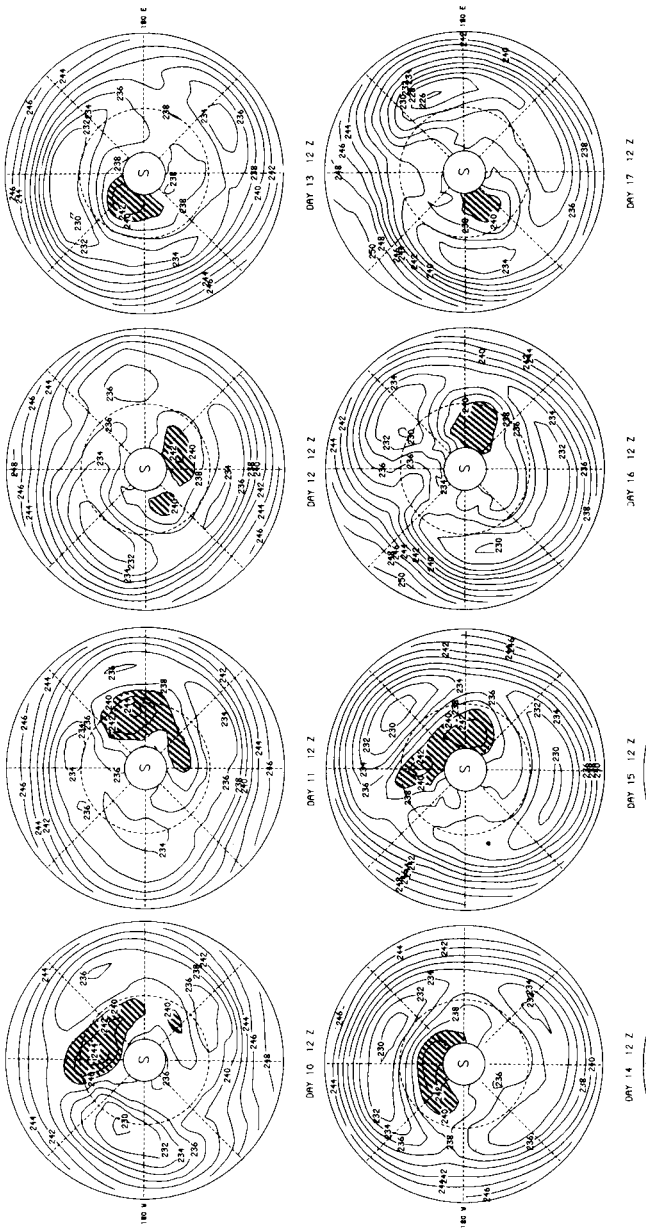


**Fig. 4.12.** Polar stereographic plot of temperature (K) at about 42 km altitude in the southern hemisphere for July 10–19, 1973 (from SCR Channel B12 radiances). Outer circle, 50°S; inner circle, 80°S; dashed circle, 60°S. Greenwich meridian at top. [After Prata (1984).]

Although the waves discussed in this section are not sustained by traveling forcing effects, some mechanism must still excite them initially, and perhaps repeatedly, so as to overcome dissipation and vertical leakage. Possibilities include stochastic forcing by latent heating, random disturbances in the atmosphere, or fluctuations of the mean winds. The waves may also be coupled to barotropic or baroclinic instabilities of matching phase speeds (see Section 5.5.2), although this coupling process has not yet been studied in detail.

## 4.5 Forced Planetary Waves

Some of the most important large-scale wave disturbances to be observed in the middle atmosphere are examples of forced planetary waves. The behavior of these waves is significantly different from that of the free planetary waves described in Section 4.4 and the propagating solar-forced tidal gravity waves of Section 4.3. In this section we present the basic theory of these forced planetary waves; observational details and interpretation are given in Chapter 5.

For simplicity we use beta-plane, rather than spherical, geometry and work with quasi-geostrophic theory, which is obeyed by these waves to a good approximation. We suppose the waves to be propagating on a basic zonal flow $[\bar{u}(y, z), 0, 0]$; the linearized potential vorticity equation is then

$$\left(\frac{\partial}{\partial t} + \bar{u}\frac{\partial}{\partial x}\right) q' + v'\bar{q}_y = Z', \tag{4.5.1}$$

where $Z'$ here denotes the nonconservative terms on the right of Eq. (3.4.5),

$$q' = \psi'_{xx} + \psi'_{yy} + \rho_0^{-1}(\rho_0 \varepsilon \psi'_z)_z \tag{4.5.2}$$

is the disturbance quasi-geostrophic potential vorticity [cf. Eq. (3.4.7)],

$$v' = \psi'_x \tag{4.5.3}$$

is the northward geostrophic wind, and

$$\bar{q}_y = \beta - \bar{u}_{yy} - \rho_0^{-1}(\rho_0 \varepsilon \bar{u}_z)_z \tag{4.5.4}$$

is the basic northward quasi-geostrophic potential vorticity gradient [which by Eq. (3.8.10) can also be related to the basic northward isentropic gradient of Ertel's potential vorticity].

Most planetary (or Rossby) waves in the stratosphere and mesosphere appear to propagate upward from forcing regions in the troposphere, and a useful way to model their middle atmosphere behavior is to consider quasi-geostrophic disturbances forced from below by fluctuations in the

height of some isobaric surface, $p = p_0$ say, which could be located in the upper troposphere or lower stratosphere (e.g., $p = 100$ mb). For simplicity, we take $p_s = p_0$ in this section (rather than $p_s = 1000$ mb: see Section 1.1.1), so that $z_0 \equiv -H \ln(p_0/p_s) = 0$. The relevant lower boundary condition is the disturbance part of Eq. (3.1.6b), which can be written in terms of $\psi' = f_0^{-1}\Phi'$ as

$$\psi' = \psi_0'(x, y, t) \qquad \text{at} \quad z = 0, \tag{4.5.5}$$

where the forcing function $\psi_0'$ is prescribed. For simplicity we for the moment consider a "channel" between vertical walls at $y = 0, L$, with lateral boundary conditions:

$$v' = \psi_x' = 0 \qquad \text{at} \quad y = 0, L. \tag{4.5.6}$$

As in Section 4.3.3, the upper boundary condition is examined case by case.

### 4.5.1 $\bar{u}$ Depends on $z$ Alone

A natural case to study first is that in which $\bar{u} = \bar{u}(z)$ and thus $\bar{q}_y = \beta - \rho_0^{-1}(\rho_0 \varepsilon \bar{u}_z)_z = \bar{q}_y(z)$. We take the nonconservative term $Z' = 0$, and suppose that the forcing is given by

$$\psi_0' = \text{Re}\, \hat{\psi}_0 e^{ik(x-ct)} \sin ly. \tag{4.5.7}$$

This has the form of a wavy pattern of zonal wavelength $2\pi k^{-1}$ and meridional wavelength $2\pi l^{-1}$, moving zonally with phase speed $c$ (eastward if $c > 0$, westward if $c < 0$). Note that $k$ is related to the spherical integer zonal wavenumber $s$ by $s = ka \cos\phi$; moreover, $\omega \equiv ck = 2\Omega\sigma$ [cf. Eq. (4.2.8)]. For consistency with the forcing, we look for solutions to Eq. (4.5.1) of the form

$$\psi' = \text{Re}\, \hat{\psi}(z) e^{ik(x-ct)} \sin ly, \tag{4.5.8}$$

which satisfies the lower boundary condition of Eq. (4.5.5) if $\hat{\psi}(0) = \hat{\psi}_0$ and the lateral boundary condition of Eq. (4.5.6) if $lL\pi^{-1}$ is an integer. [Alternatively, we can replace $\sin ly$ by 1 in Eqs. (4.5.7) and (4.5.8).] Substitution of Eq. (4.5.8) into Eq. (4.5.1) and use of Eqs. (4.5.2,3) lead to the following second-order ordinary differential equation for $\hat{\psi}(z)$:

$$\rho_0^{-1}(\rho_0 \varepsilon \hat{\psi}_z)_z + \left[\frac{\bar{q}_y(z)}{\bar{u}(z) - c} - (k^2 + l^2)\right]\hat{\psi} = 0 \tag{4.5.9}$$

with lower boundary condition

$$\hat{\psi} = \hat{\psi}_0 \qquad \text{at} \quad z = 0 \tag{4.5.10}$$

and an upper boundary condition to be determined.

If $\bar{u}(z) = c$ at some level $z = z_c$—the *critical level*—the coefficient of $\hat{\psi}$ in Eq. (4.5.9) is infinite there if $\bar{q}_y(z_c) \neq 0$. In such a case it is known from the theory of differential equations that $\hat{\psi}$ is generally logarithmically infinite at $z_c$ if $\bar{u}_z(z_c) \neq 0$; extra physics, such as transience, dissipation, or nonlinearity, must be included in the theory if this infinity is to be avoided. Critical levels are the subject of much current research, and are mentioned again in Section 4.5.4 and also in Section 5.6.

### 4.5.2 *Constant $\bar{u}$ and $N$*

To gain some insight into the nature of solutions of Eq. (4.5.9), we specialize still further, by taking $\bar{u}$ constant, so that $\bar{q}_y = \beta$ = constant and $N$ constant, so that $\varepsilon$ is constant. Then Eq. (4.5.9) can be written

$$\hat{\psi}_{zz} - H^{-1}\hat{\psi}_z + B\hat{\psi} = 0$$

where

$$B = \varepsilon^{-1}\left[\frac{\beta}{\bar{u} - c} - (k^2 + l^2)\right], \tag{4.5.11}$$

since $\rho_0 = \rho_s e^{-z/H}$. Looking for solutions $\hat{\psi} \propto e^{\Lambda z}$, we find

$$\Lambda = \frac{1}{2H} \pm \left(\frac{1}{4H^2} - B\right)^{1/2}.$$

Two possibilities arise, according as the term inside the square root is positive or negative:

#### 1. $(1/4H^2) - B \equiv \nu^2 > 0$

In this case $\Lambda = (2H)^{-1} \pm \nu$ where $\nu = +[(1/4H^2) - B]^{1/2}$, and $\hat{\psi} = \hat{\psi}_0 \exp[(z/2H) \pm \nu z]$ or $\rho_0^{1/2}\hat{\psi} = \rho_s^{1/2}\hat{\psi}_0 e^{\pm \nu z}$. The wave activity density $A = \frac{1}{2}\rho_0 q'^2/\bar{q}_y$, noted in Section 3.6 as a natural measure of wave amplitude when $\bar{q}_y > 0$ will then vary with height as $e^{\pm 2\nu z}$; the wave energy per unit volume, as given by the term $\frac{1}{2}\rho_0(\overline{u'^2} + \overline{v'^2} + \overline{\Phi_z'^2}/N^2)$ in Eq. (3.6.3), will do likewise. Clearly the appropriate upper boundary condition is that quantities like these should be bounded as $z \to \infty$, and the lower sign must be selected. (In fact $A$ and the wave-energy density then vanish as $z \to \infty$.) Thus

$$\psi' = \psi_0'(x, y, t) \exp\left(\frac{1}{2H} - \nu\right) z;$$

this is an example of a trapped, or edge, wave, and has no phase tilt with height. Note that $\psi'$, $u'$, $v'$, etc., actually grow with height if $\nu < 1/2H$, that is, if $B > 0$; however, the decreasing basic density $\rho_0$ more than compensates for this in the wave-activity or wave-energy density.

*2.* $(1/4H^2) - B \equiv -m^2 < 0$

In this case we can put $\Lambda = (2H)^{-1} + im$, where

$$m = \pm\left(B - \frac{1}{4H^2}\right)^{1/2} \tag{4.5.12}$$

and

$$\psi' = \text{Re}\,\hat{\psi}_0 \exp\left[\frac{z}{2H} + i(kx + mz - kct)\right] \sin ly. \tag{4.5.13}$$

The presence of $imz$ in the exponential here indicates vertical wave propagation, and phase lines tilt with height. The solution, Eq. (4.5.13), represents a Rossby wave propagating vertically and zonally. Eliminating $B$ from Eqs. (4.5.11,12), we obtain the equation

$$\bar{u} - c = \beta[k^2 + l^2 + \varepsilon(m^2 + 1/4H^2)]^{-1}; \tag{4.5.14}$$

in this case where $0 < m^2 < \infty$ and $\beta$, $k^2$, $l^2$, $\varepsilon$, and $H^2$ are all positive, we obtain the criterion

$$0 < \bar{u} - c < \bar{u}_c \equiv \beta(k^2 + l^2 + \varepsilon/4H^2)^{-1} \tag{4.5.15}$$

(Charney and Drazin, 1961). For waves whose phase is stationary with respect to the ground, with $c = 0$, we have

$$0 < \bar{u} < \bar{u}_c \tag{4.5.16}$$

for vertical propagation; thus for this case of constant $\bar{u}$ and $N$, "stationary" vertically propagating Rossby waves can only exist in winds that are westerly (eastward) and not too strong.

It should be noted that the limiting speed $\bar{u}_c$ depends on the zonal and meridional wave numbers of the mode in question. For a typical stratospheric static stability ($N^2 = 5 \times 10^{-4}\ \text{s}^{-2}$), and choosing $l = \pi/(10{,}000\ \text{km})$, we find at 60°N

$$\bar{u}_c \approx 110/(s^2 + 3) \quad \text{m s}^{-1}$$

where the integer $s = ka \cos\phi$ is the spherical zonal wave number, as above. Thus on the basis of this very simple model, wave number 1 ($s = 1$) propagates in westerlies weaker than about $28\ \text{m s}^{-1}$, wave number 2 in westerlies weaker than about $16\ \text{m s}^{-1}$, and so on. Of course this model

cannot hope to represent very faithfully the propagation of such global-scale modes in realistic mean zonal shear flows, but it does illustrate the fact that the "window" for propagation given by Eq. (4.5.16) becomes smaller as the zonal wave number $s$ increases. This is in broad agreement with observations, which show that stationary disturbances tend to be composed only of the "ultralong" Fourier components $s = 1, 2, 3$ in the winter westerlies and tend to be absent in the stratospheric easterlies (see Chapter 5). More sophisticated theories, involving more general basic states and forms of disturbance, will be mentioned in Sections 4.5.4 and 5.3.

It remains to determine the sign of $m$ in Eq. (4.5.12); here the radiation condition must be used, as in Section 4.3.3, since the wave-activity density and wave-energy density are both constant with height, irrespective of the sign of $m$. We again compute the vertical group velocity $c_g^{(z)}$ and choose it to be positive, in accordance with the general belief that planetary waves normally propagate upward from the troposphere into the stratosphere, rather than downwards.

To calculate $c_g^{(z)}$ we rearrange Eq. (4.5.14) so as to obtain the Rossby wave dispersion relation in the form

$$\omega \equiv ck = k\bar{u} - \beta k[k^2 + l^2 + \varepsilon(m^2 + 1/4H^2)]^{-1} \tag{4.5.17}$$

so that

$$c_g^{(z)} \equiv \frac{\partial \omega}{\partial m} = 2\varepsilon\beta km[k^2 + l^2 + \varepsilon(m^2 + 1/4H^2)]^{-2}. \tag{4.5.18}$$

Taking $k > 0$ by convention we see that $c_g^{(z)}$ is positive if $m > 0$, and so the upper sign must be chosen in Eq. (4.5.12). The phase surfaces, $kx + mz - kct$ = constant, thus tilt westward with height, as observed for planetary waves in the stratosphere.[2] For stationary waves, we put $c = \omega = 0$ after calculating $\partial\omega/\partial m$; although the phase surfaces for such waves are fixed in space, the waves still transfer information vertically.

An alternative method of motivating the choice of $m$ is to include small dissipative terms. A simple model uses Newtonian cooling and Rayleigh friction with equal, constant, rate coefficients $\delta > 0$, so that $(X', Y', Q') = \delta(u', v', \theta')$; it can then be shown that $Z' = -\delta q'$ in Eq. (4.5.1). In the stationary-wave case, for example, it follows that $\bar{u}\,\partial/\partial x$ is replaced by $\bar{u}\,\partial/\partial x + \delta$, and we find $\hat{\psi} \propto e^{\Lambda z}$, where

$$\Lambda \approx \frac{1}{2H} \pm \left(\frac{1}{4H^2} - B - \frac{i\,\delta\beta}{\varepsilon k\bar{u}^2}\right)^{1/2}$$

[2] Note that if $k$ is chosen negative then the group velocity condition implies that $m$ must also be negative, and the phase tilt is still westward with height. All other physical properties of the wave solution are likewise unaltered.

if $\delta \ll |k\bar{u}|$ and $B$ is as defined before. In case (2) above, this yields

$$\Lambda \approx \frac{1}{2H} - \frac{\delta\beta}{2\varepsilon k\bar{u}^2 m} + im$$

where $m$ is given by Eq. (4.5.12) and

$$\psi' = \text{Re}\,\hat{\psi}_0 \exp\left[\frac{z}{2H} - \frac{\delta\beta z}{2\varepsilon k\bar{u}^2 m} + i(kx + mz)\right] \sin ly.$$

Thus small dissipation produces an extra factor $\exp(-\delta\beta z/2\varepsilon k\bar{u}^2 m)$, which implies that the wave-activity or wave-energy density decreases with $z$ if $m > 0$, given the convention $k > 0$ as before. Letting $\delta \to 0$ we obtain the same choice of sign of $m$ for the conservative case as given by the group velocity argument presented above.

We note finally that when $N$ is constant, the vertical wave number $m$ used here is given in terms of the equivalent depth $h$ used in Sections 4.2 and 4.3 by

$$m^2 = (N^2/gh) - 1/4H^2 \tag{4.5.19}$$

[cf. Eq. (4.3.6)]; thus $m^2$ equals the coefficient of $W$ in the vertical structure equation [Eq. (4.2.7a)]. When $\bar{u} = 0$, Eq. (4.5.17) can be written

$$\frac{\omega}{k} = -\beta(k^2 + l^2 + f_0^2/gh)^{-1}$$

using Eqs. (4.5.19) and (3.2.16), and as $h \to \infty$ this approaches the spherical version of Eq. (4.2.14b) for the same limit, if the definitions $\beta = 2\Omega a^{-1}\cos\phi$ and $s = ka\cos\phi$ are used and $k^2 + l^2$ replaced by its spherical analog $n_R(n_R + 1)a^{-2}$.

### 4.5.3 *Fluid Parcel Orbits and the Stokes Drift for Rossby Waves*

As well as being a useful idealized model of a propagating planetary wave in the winter stratosphere, the solution of Eq. (4.5.13) is also convenient for didactic purposes. We use it here to illustrate some of the Lagrangian concepts mentioned in Section 3.7.

For simplicity we consider stationary waves ($c = 0$), so that the uniform basic flow $\bar{u}$ is westerly and satisfies Eq. (4.5.16); we also choose the width of the channel $L$ to equal $\pi l^{-1}$, so that $\sin ly$ has a single peak in midchannel. If $\hat{\psi}_0$ is taken to be real, Eq. (4.5.13) becomes

$$\psi' = \hat{\psi}_0 e^{z/2H} \cos(kx + mz) \sin ly. \tag{4.5.20}$$

The geostrophic velocities are

$$u' = -\psi'_y = -l\hat{\psi}_0 e^{z/2H} \cos(kx + mz) \cos ly, \tag{4.5.21a}$$

$$v' = \psi'_x = -k\hat{\psi}_0 e^{z/2H} \sin(kx + mz) \sin ly \tag{4.5.21b}$$

[cf. Eq. (3.5.9)]. Using Eqs. (3.2.11) and (3.2.12) with $Q = 0$ we obtain the adiabatic quasi-geostrophic relationship

$$w_a = -D_g\left(\frac{f_0\psi_z}{N^2}\right),$$

which on linearization in the present case gives

$$w' = -\frac{\bar{u}f_0\psi'_{zx}}{N^2}, \tag{4.5.22}$$

since the waves are stationary ($\partial/\partial t = 0$) and since $\bar{\psi}_{zy} = -\bar{u}_z = 0$. We drop the subscript a on $w'$ for convenience.

The definitions in Eqs. (3.7.1) of parcel displacements $(\xi', \eta', \zeta')$ reduce to

$$\bar{u}\frac{\partial}{\partial x}(\xi', \eta', \zeta') = (u', v', w') \tag{4.5.23a,b,c}$$

here, and so

$$\xi' = -\frac{l}{k\bar{u}}\hat{\psi}_0 e^{z/2H} \sin(kx + mz) \cos ly, \tag{4.5.24a}$$

$$\eta' = \frac{1}{\bar{u}}\hat{\psi}_0 e^{z/2H} \cos(kx + mz) \sin ly. \tag{4.5.24b}$$

From Eqs. (4.5.22), (4.5.23c), and (4.5.20), we obtain

$$\begin{aligned}\zeta' &= -\frac{f_0\psi'_z}{N^2} \\ &= -\frac{f_0}{N^2}\hat{\psi}_0 e^{z/2H}\left[\frac{1}{2H}\cos(kx + mz) - m \sin(kx + mz)\right] \sin ly.\end{aligned} \tag{4.5.24c}$$

The "constants" of $x$ integration have been set to zero, in accordance with Eq. (3.7.2). Trajectories or orbits of parcels correct to the linear approximation, as viewed moving with the basic zonal flow $\bar{u}$, are shown in Fig. 4.13; their projections in the $xy$ and $yz$ planes are ellipses.

Knowledge of the parcel displacements of Eqs. (4.5.24) allows us to calculate quantities like the Stokes drift velocities $(\bar{u}^S, \bar{v}^S, \bar{w}^S)$. From Eq.

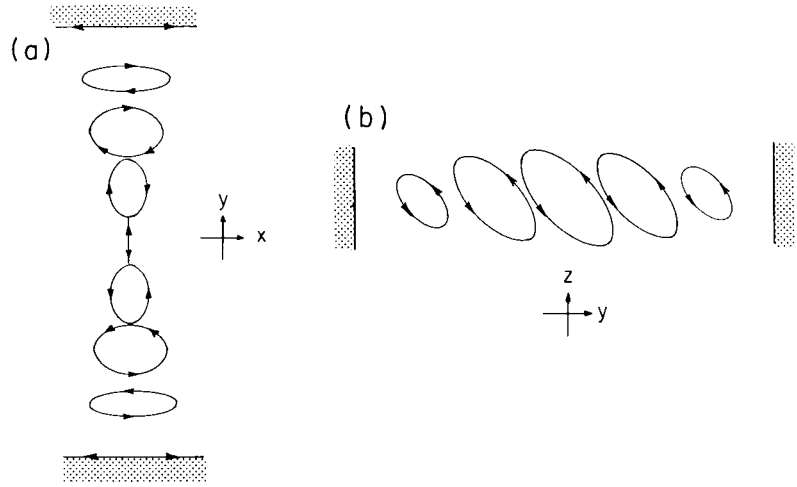


**Fig. 4.13.** Orbits of fluid parcels disturbed by a Rossby wave, correct to first order in wave amplitude, as viewed moving with the mean flow. (a) Projection of orbits in the $xy$ plane. (b) Projection of orbits in the $yz$ plane. [Adapted from Matsuno (1980), Birkhäusen Verlag AG, Basle, Switzerland.]

(3.7.7) we have $\bar{u}^S = \overline{\boldsymbol{\xi}' \cdot \nabla u'} + O(\alpha^3)$, since $\bar{u}$ is constant to $O(\alpha^0)$; thus, using Eq. (3.7.4) and the fact that zonal averages are independent of $x$, we obtain

$$\bar{u}^S = \rho_0^{-1} \nabla \cdot (\rho_0 \overline{\boldsymbol{\xi}' u'}) = (\overline{\eta' u'})_y + \rho_0^{-1} (\rho_0 \overline{\zeta' u'})_z. \tag{4.5.25a}$$

In a rather similar manner we have

$$\bar{v}^S = (\overline{\eta' v'})_y + \rho_0^{-1} (\rho_0 \overline{\zeta' v'})_z, \tag{4.5.25b}$$

$$\bar{w}^S = (\overline{\eta' w'})_y + \rho_0^{-1} (\rho_0 \overline{\zeta' w'})_z. \tag{4.5.25c}$$

Using Eqs. (4.5.21), (4.5.22), and (4.5.24), we then obtain for the present case

$$\bar{u}^S = -\frac{l^2}{2\bar{u}} \hat{\psi}_0^2 e^{z/H} \cos 2ly, \qquad \bar{v}^S = 0,$$

$$\bar{w}^S = \frac{f_0 klm}{2N^2} \hat{\psi}_0^2 e^{z/H} \sin 2ly,$$

after a short calculation, which is expedited by using results like $\overline{\eta' v'} = \bar{u} \eta' \eta'_x = \bar{u} (\frac{1}{2} \eta'^2)_x = 0$, from Eq. (4.5.23b). Thus the zonal Stokes drift $\bar{u}^S$ is directed eastward in midchannel ($L/4 < y < 3L/4$) and westward elsewhere, while the vertical Stokes drift $\bar{w}^S$ is upward in the southern half of the channel ($0 < y < L/2$) and downward in the northern half ($L/2 < y < L$).

It must be recalled, however, that the Stokes drift represents the difference between the Lagrangian-mean flow and the Eulerian-mean flow. Under the present "nonacceleration conditions," we can use the Charney-Drazin theorem of Section 3.6 to infer that $\bar{v}^* = \bar{w}^* = 0$ under appropriate boundary conditions, and hence to show that $\bar{v} = 0$ and $\bar{w} = -\bar{w}^S$ by Eq. (3.5.1) and manipulations similar to those used above. Thus $\bar{v}^L = \bar{w}^L = 0$ here, consistent with the GLM nonacceleration theorem mentioned in Section 3.7.1. However, the computation of $\bar{u}^L$ to second order in the wave amplitude $\alpha$ involves consideration of how the flow is initially set up, and requires a much more detailed analysis than the calculations based on the steady linear solutions that have been presented here.

### 4.5.4 *Steady Planetary Waves in More General Basic States*

For detailed comparison of linear theory with the observed middle atmosphere, the restriction to mean zonal flows $\bar{u}$ that are constant, or depend on $z$ alone, is rather unsatisfactory. We therefore now consider basic flows $\bar{u}$ that depend on $y$ and $z$, although we shall still take $N$, and thus $\varepsilon$, to be constant. The latter restriction can easily be relaxed, at the expense of a little extra algebra.

Returning to Eqs. (4.5.1)-(4.5.3), setting $Z' = 0$ and substituting the steady-wave form

$$\psi' = e^{z/2H} \operatorname{Re}[\Psi(y, z)e^{ik(x-ct)}] \tag{4.5.26}$$

we obtain

$$\Psi_{yy} + \varepsilon\Psi_{zz} + n_k^2\Psi = 0, \tag{4.5.27}$$

where

$$n_k^2(y, z) = (\bar{u} - c)^{-1}\bar{q}_y - k^2 - \varepsilon/4H^2, \tag{4.5.28}$$

(Dickinson, 1968). The quantity $n_k^2$ is the square of the *refractive index*, for zonal wave number $k$ and phase speed $c$. In "stretched" coordinates $(\tilde{y}, \tilde{z}) \equiv (y, \varepsilon^{-1/2}z)$, Eq. (4.5.27) is identical to the equation for two-dimensional sound, or light, waves in a medium of varying refractive index, and we can use insights from the theory of acoustics or optics. In particular, we expect waves to propagate in regions where $n_k^2 > 0$ and to avoid regions where $n_k^2 < 0$. Note that $n_k^2$ depends on the two-dimensional structure of $(\bar{u} - c)^{-1}\bar{q}_y$, as well as on $k^2$, so that propagation generally depends on more complex criteria than the simple Charney-Drazin condition [Eq. (4.5.15)] that applies when $\bar{u}$ and $\bar{q}_y$ (and thus $n_k^2$) are constant. Note also that $n_k^2$ generally becomes infinite at a *critical line* (or *critical surface*) where $\bar{u}(y, z) = c$; as for the critical level, mentioned above for the case $\bar{u} = \bar{u}(z)$, such surfaces need special attention.

Given suitable boundary conditions, Eq. (4.5.27) or its spherical-geometry equivalent is readily amenable to numerical solution for realistic flows $\bar{u}(y, z)$, and a number of studies of this sort have been carried out, following Matsuno (1970). Some examples of calculations, and comparison with observed planetary waves, will be mentioned in Section 5.3; we shall here just discuss some semianalytical methods that can be used to solve special cases of Eq. (4.5.27).

The first of these is applicable when $\bar{u} = \bar{u}(y)$, so that $n_k^2$ depends on $y$ alone; separable solutions $\Psi^{(l)}(y, z) = \Psi_l(y)e^{im_l z}$ to Eq. (4.5.27) can be sought, where

$$\frac{d^2\Psi_l}{dy^2} + [n_k^2(y) - \varepsilon m_l^2]\Psi_l = 0, \qquad l = 1, 2, \ldots$$

is solved as an eigenvalue problem, subject to suitable lateral boundary conditions, say $\Psi_l = 0$ at $y = 0, L$. The eigenvalues $m_l^2$ give the vertical structure—propagating if $m_l^2 > 0$, trapped if $m_l^2 < 0$. The analysis is similar to that of Section 4.5.2, and the response to a given lower boundary forcing can be found in terms of a sum of modes $\Psi^{(l)}$.

The assumption $\bar{u} = \bar{u}(y)$ and the imposition of vertical walls at $y = 0, L$ are, however, rather unrealistic, since they tend to confine wave propagation to the vertical, and thus inhibit latitudinal propagation. Observations of middle atmosphere planetary waves, on the other hand, suggest that latitudinal propagation is very significant in many cases: see Section 5.3. A popular approach for analyzing such cases, with $n_k^2$ varying with $y$ and $z$, is to use an approximate theory, analogous to "geometric optics," to investigate Eq. (4.5.27). It is called the *WKBJ* or Liouville-Green method; a brief outline of the theory is given in Appendix 4A. In the present case one supposes that

$$\Psi = \hat{\Psi}(y, z) \exp i\chi(y, z)$$

where the phase $\chi$ is real, and varies much more rapidly with $y$ and $z$ than do the basic-flow quantities $\bar{u}$, $\bar{q}_y$, or $n_k^2$, the amplitude $\hat{\Psi}$, or the derivatives of $\chi$. This is equivalent to looking for locally sinusoidal solutions whose $y$ and $z$ wavelengths are much less than typical $y$ and $z$ scales of the basic flow. The theory can be formalized, if desired, in terms of a small "*WKBJ* parameter," say $\mu_w$, characterizing the ratio of these wavelengths to the meridional scales of the basic flow; it requires that $n_k^2 L_0^2 \geq O(\mu_w^{-2})$, where $L_0$ is a typical horizontal mean-flow scale or $\varepsilon^{-1/2}$ times a typical vertical mean-flow scale.

Under these assumptions, one can *define* local meridional wave numbers

$$l \equiv \partial\chi/\partial y, \qquad m \equiv \partial\chi/\partial z,$$

and to leading order in $\mu_w$ it is found that $\Psi_{yy} \approx -l^2\Psi$, $\Psi_{zz} \approx -m^2\Psi$. Thus Eqs. (4.5.27) and (4.5.28) yield an approximate dispersion relation for $\omega = ck$, analogous to Eq. (4.5.17):

$$\omega = \Delta(k, l, m; y, z) \equiv k\bar{u}(y, z) - k\bar{q}_y(y, z)[k^2 + l^2 + \varepsilon(m^2 + 1/4H^2)]^{-1} \tag{4.5.29}$$

and local group velocity components

$$c_g^{(y)} \equiv \partial\Delta/\partial l, \qquad c_g^{(z)} \equiv \partial\Delta/\partial m, \tag{4.5.30}$$

giving the local paths of propagation of information—the *rays*—in the $yz$ plane. Standard *ray-tracing equations* can then be used to compute how the local wave numbers vary along a ray; for example, it can be shown that the variation of the vertical wavenumber along a ray is given by

$$\left[c_g^{(y)}\frac{\partial}{\partial y} + c_g^{(z)}\frac{\partial}{\partial z}\right]m = -\frac{\partial\Delta}{\partial z} \tag{4.5.31}$$

[where the $z$ derivative on the right acts only on the terms $\bar{u}$ and $\bar{q}_y$ in Eq. (4.5.29) where $z$ appears explicitly]. Using numerical methods, and given suitable "initial" conditions, the ray-tracing equations can be solved to find the paths of propagation through realistic stratospheric and mesospheric wind structures $\bar{u}(y, z)$. An extension of the approach also allows the calculation of amplitude variations along the rays: further details are mentioned in Appendix 4A. Because of the large latitudinal excursion of many of the rays, such calculations are best carried out with full allowance for the spherical geometry of the earth, rather than on a beta-plane. A typical example of a ray-tracing calculation is shown in Fig. 4.14a and the corresponding $\bar{u}$ and $n_k^2(y, z)$ are contoured in Figs. 4.14b,c. The most prominent feature of the rays is their tendency to be deflected up the gradient of $n_k^2$, and thus equatorward. This gradient depends partly on the variation of $\beta = 2\Omega a^{-1}\cos\phi$ with latitude $\phi$, and is present even when $\bar{u}$ (or, rather, the angular velocity, on the sphere) is constant; however, it is greatly enhanced by variations in $(\bar{u} - c)^{-1}$ when the latter becomes large near a critical line, such as that present in low latitudes in Figs. 4.14b,c. Whether rays are absorbed or reflected at these critical lines in still a matter for investigation: see Section 5.6.

Despite the approximations involved, this *WKBJ* theory has provided useful insights into the propagation of planetary waves in the observed middle atmosphere and in more complex models such as the detailed linear numerical models described in Sections 5.3 and 6.3 and the general circulation models outlined in Chapter 11. It is also possible that an extension of the method might be of value for the investigation of disturbances to basic states that are not zonally symmetric.

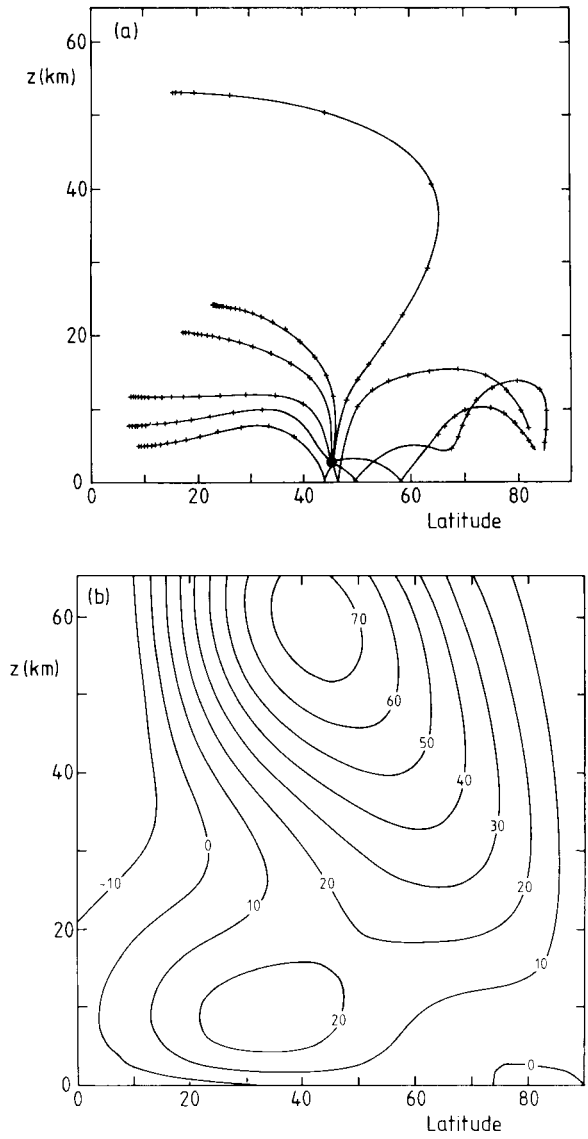


**Fig. 4.14.** Calculations of the propagation of stationary Rossby waves in an idealized northern hemisphere winter basic state. (a) Rays for zonal wave number 1, starting at 45°N and $z \approx 3$ km, with crosses marked at daily time intervals. (b) Basic zonal wind $\bar{u}(\phi, z)$ in m s$^{-1}$. (c) Spherical analog of $a^2 n_k^2 \cos^2 \phi$ for the wind field given in (b), where $k$ corresponds to zonal wave number $s = 1$. Region of negative $n_k^2$ is shaded, and solid contours are spaced at unit intervals in the quantity $(a^2 n_k^2 \cos^2 \phi + 1)^{1/2}$. The closely packed contours at low latitudes indicate the presence of a critical line. [Adapted from Karoly and Hoskins (1982).]

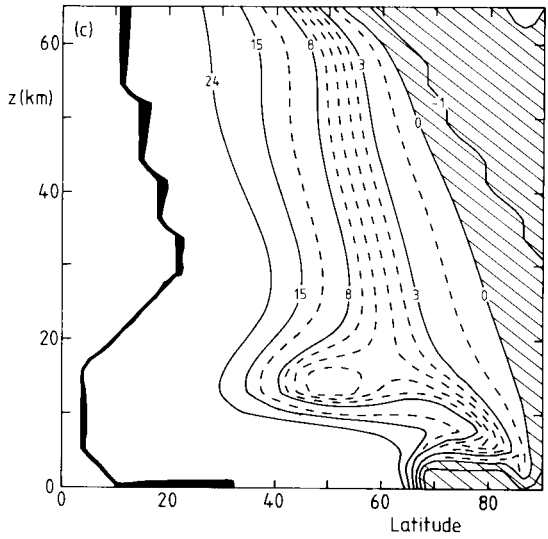


**Fig. 4.14** (*continued*)

### *4.5.5 The Eliassen-Palm Flux for Forced Rossby Waves*

The Eliassen-Palm (EP) flux was introduced in Sections 3.5 and 3.6, where its importance in the theory of wave, mean-flow interaction was described. It is of interest to calculate this quantity for the planetary waves discussed above; to this end it is convenient to rewrite the quasi-geostrophic beta-plane version of **F**,

$$\mathbf{F} = (0, -\rho_0 \overline{v'u'}, \rho_0 f_0 \overline{v'\theta'}/\theta_{0z})$$

[cf. Eq. (3.5.6)], in the form

$$\mathbf{F} = (0, \rho_0 \overline{\psi'_x \psi'_y}, \rho_0 \varepsilon \overline{\psi'_x \psi'_z}), \tag{4.5.32}$$

using Eqs. (3.2.3), (3.2.12), and (3.2.16).

We first consider the simple solutions of Section 4.5.2, where $\bar{u}$ and $N$ are constant, and the stream function has "modal" latitudinal structure, proportional to $\sin ly$. In the absence of dissipation it is easy to verify that in the "trapped" case (1) $\mathbf{F} \equiv \mathbf{0}$, while in the "vertically propagating" case (2) $\mathbf{F} = (0, 0, \frac{1}{2}\rho_s \varepsilon mk |\hat{\psi}_0|^2 \sin^2 ly)$ and points vertically upward. In each case $\nabla \cdot \mathbf{F} = \partial F^{(z)}/\partial z = 0$, as is to be expected from the Eliassen-Palm theorem [Eq. (3.6.1)], since these waves are steady, conservative, and linear; they thus induce no mean-flow acceleration (see Sections 3.6 and 4.1). On the other hand, if dissipation is included, such as the weak Rayleigh friction

and Newtonian cooling considered in Section 4.5.2, $\nabla \cdot \mathbf{F}$ is found to be negative in general, and "nonacceleration conditions" are violated.

It is also straightforward to calculate $\mathbf{F}$ for the approximate *WKBJ* solutions of Section 4.5.4; we find

$$\mathbf{F} \approx \tfrac{1}{2}\rho_s k |\hat{\Psi}|^2 (0, l, \varepsilon m), \tag{4.5.33}$$

while the wave-activity density $A = \frac{1}{2}\rho_0 \overline{q'^2}/\bar{q}_y$ [cf. Eq. (3.6.6)] is given by

$$A \approx \tfrac{1}{4}\rho_s (k^2 + l^2 + \varepsilon m^2)^2 |\hat{\Psi}|^2 / \bar{q}_y, \tag{4.5.34}$$

since $q' \approx -(k^2 + l^2 + \varepsilon m^2)\psi'$ under *WKBJ* conditions, from Eq. (4.5.2). It can further be verified that

$$\mathbf{F} = (0, c_g^{(y)}, c_g^{(z)}) A \tag{4.5.35}$$

to leading order in $\mu_w$ for these waves, using Eqs. (4.5.29), (4.5.30), (4.5.33), and (4.5.34). Thus $\mathbf{F}$ is parallel or antiparallel to the group velocity at each point under these conditions—and therefore to the rays defined in Section 4.5.4—according as $A > 0$ or $A < 0$. Note that in the present quasi-geostrophic case $A$ has the same sign as $\bar{q}_y$, by Eqs. (3.6.6) or (4.5.34)—this is usually positive in the midlatitude stratosphere and mesosphere.

Following standard practice, the group velocity and the concept of a ray have been defined above only in the context of a *WKBJ* theory of almost-sinusoidal waves. However, Eq. (4.5.35) suggests that, in more general situations where the *WKBJ* approximations fail, one possible extended definition of the group velocity is

$$\mathbf{C} \equiv \mathbf{F}/A, \tag{4.5.36}$$

where $\mathbf{F}$ and $A$ are given by Eqs. (3.5.6) and (3.6.6), respectively, or their primitive-equation equivalents. Generalized "rays" can then be defined as curves parallel to $\mathbf{C}$ at every point. These ideas will be used in Chapters 5 and 6 for interpreting the behavior of planetary waves in the atmosphere and in models.

## 4.6 Gravity Waves

It was mentioned in Section 4.1 that pure internal gravity waves owe their existence to buoyancy restoring forces, while inertio-gravity waves are due to the combined effects of buoyancy and Coriolis forces. The "gravity modes" identified in Figs. 4.2a,b, which include the main propagating tidally forced modes of Section 4.3, are, strictly speaking, examples of inertio-gravity waves, since they are generally affected to some extent by the rotation of the earth. In the present section we consider some rather simpler gravity

waves, restricting attention to waves of comparatively small scale (tens to hundreds of kilometers in horizontal wavelength), so that the complications of spherical geometry can be avoided.

Gravity waves of this scale appear to be common in the upper mesosphere, where they have been detected by radars and other instruments; for example, Fig. 4.15 shows some radar observations of internal gravity waves in this region. The periods of waves of this type are typically a few minutes to an hour or so, and vertical wavelengths range from 5 to 15 km. Although direct measurements are difficult, the waves are thought to have horizontal wavelengths of up to about 100–200 km, and horizontal phase speeds of up to 80 m $s^{-1}$. Inertio-gravity waves, with periods approaching the local "inertial period" $2\pi f^{-1}$ and vertical wavelengths on the order of 10 km, have been detected in the upper mesosphere and also in the lower stratosphere, and these can have horizontal wavelengths of over a thousand kilometers: some observations are shown in Fig. 4.16. Internal gravity waves are also likely to be common in the lower mesosphere and the stratosphere, but observations at these levels are sparse at present.

### *4.6.1 Pure Internal Gravity Waves*

We start by considering small wave disturbances about a basic state of rest, whose frequencies are large compared to the local inertial frequency $f = 2\Omega \sin \phi$. We therefore neglect the effects of the earth's rotation by putting $f = 0$ in Eq. (4.2.1), set $X' = Y' = J' = 0$, and employ Cartesian coordinates $x$ and $y$. We obtain

$$u'_t + \Phi'_x = 0, \qquad v'_t + \Phi'_y = 0, \tag{4.6.1a,b}$$

$$u'_x + v'_y + \rho_0^{-1}(\rho_0 w')_z = 0, \qquad \Phi'_{zt} + N^2 w' = 0. \tag{4.6.1c,d}$$

For simplicity we take $N$ to be constant; we then substitute

$$(u', v', w', \Phi') = e^{z/2H}\,\mathrm{Re}[(\hat{u}, \hat{v}, \hat{w}, \hat{\Phi}) \exp i(kx + ly + mz - \omega t)] \tag{4.6.2}$$

into Eq. (4.6.1), where $\hat{u}$ etc. are constant, and obtain the following equations:

$$\hat{u} = \frac{k}{\omega}\hat{\Phi}, \qquad \hat{v} = \frac{l}{\omega}\hat{\Phi}, \qquad \hat{w} = -\frac{\omega}{N^2}\left(m - \frac{i}{2H}\right)\hat{\Phi}, \tag{4.6.3a,b,c}$$

and the dispersion relation

$$\omega^2 = \frac{N^2(k^2 + l^2)}{m^2 + 1/4H^2}. \tag{4.6.4}$$

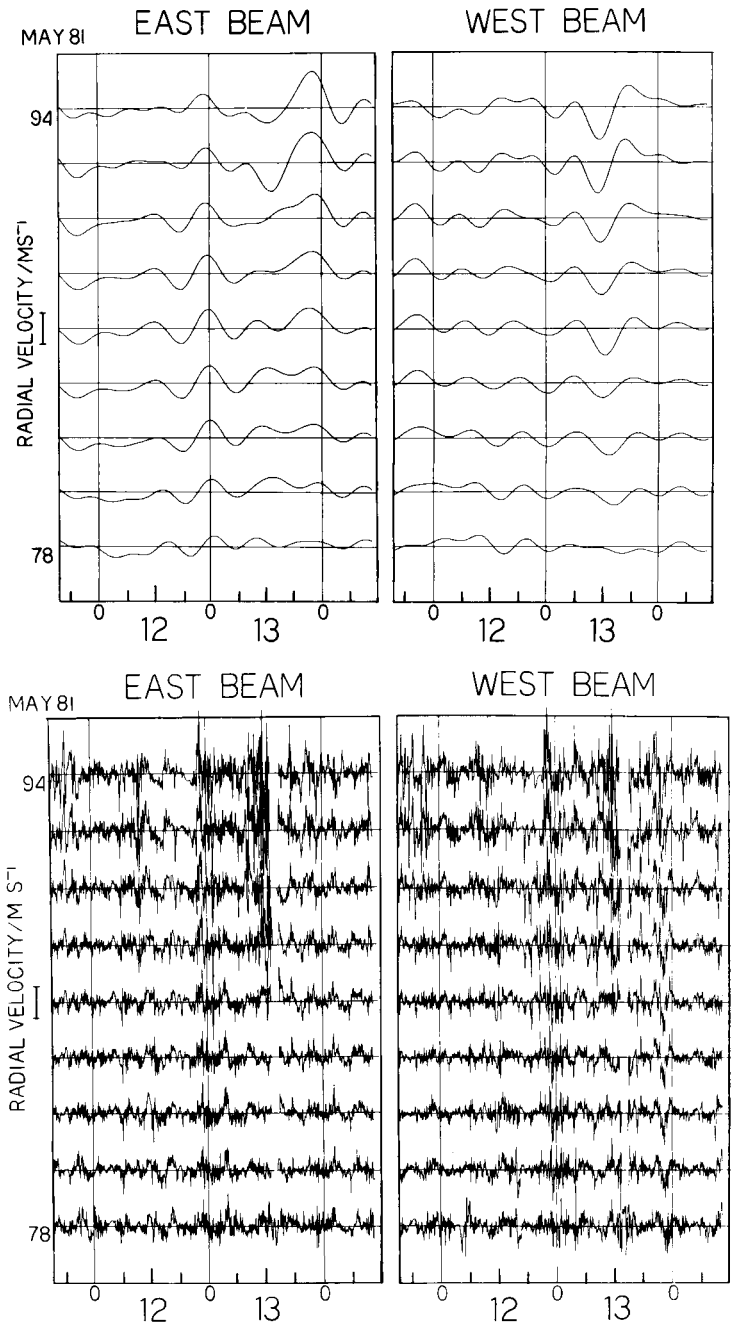


**Fig. 4.15.** High-frequency radar measurements of line-of-sight velocities at heights between 78 and 94 km in the upper mesosphere measured in two directions, equally inclined at small angles to the vertical. Top panels show data filtered to include only periods longer than 8 hr and bottom panels show data filtered to include only periods from 8 min to 8 hr. The data were collected during May 11-14, 1981. [After Vincent and Reid (1983).]

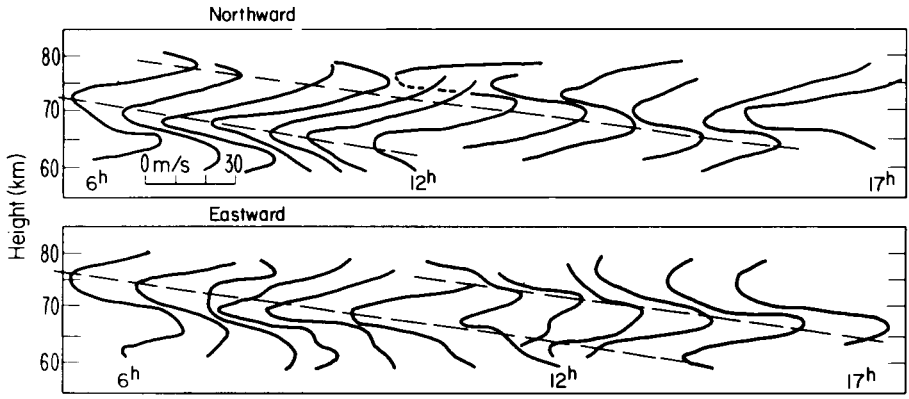


**Fig. 4.16.** Time sequence of northward and eastward velocity components as measured by very-high-frequency (VHF) radar during an unusually quasi-sinusoidal inertio-gravity wave event in the mesosphere, measured October 11, 1981, in Poker Flat, Alaska (1-hr average values). Velocity scale is shown in the lower left corner of the upper panel. Dashed lines indicate approximate height of velocity extrema and show downward phase propagation. Note that the left-to-right profile placements are not precisely uniform in time. [After Balsley *et al.* (1983). American Meteorological Society.]

Note that in terms of the equivalent depth $h$ this can be written $\omega^2 = gh(k^2 + l^2)$, using Eq. (4.5.19); this is consistent with the "nonrotating" limit $\gamma^{-1/2} \to \infty$ for gravity waves given by Eq. (4.2.14a) if $k^2 + l^2$ is replaced by its spherical equivalent $n_G(n_G + 1)a^{-2}$.

Using methods analogous to those of Section 4.5.3, it can be shown that particles move in elliptical orbits (with tilted axes) in vertical planes perpendicular to the horizontal vector $(-l, k, 0)$.

It should be noted from Eqs. (4.6.2) and (4.6.3) that

$$\rho_0 \overline{u'w'} = \tfrac{1}{2}\rho_0 \operatorname{Re}(e^{z/H}\hat{u}\hat{w}^*) = \tfrac{1}{2}\rho_s \operatorname{Re}\left[\frac{k}{\omega}\hat{\Phi}\left(\frac{-\omega}{N^2}\right)\left(m + \frac{i}{2H}\right)\hat{\Phi}^*\right]$$

$$= -\tfrac{1}{2}\rho_s \frac{mk}{N^2}|\hat{\Phi}|^2$$

where an asterisk denotes the complex conjugate. Thus $\rho_0 \overline{u'w'}$ is independent of $z$, so that

$$\rho_0^{-1}(\rho_0 \overline{u'w'})_z = 0,$$

which is the Eliassen-Palm theorem [Eq. (3.6.1)] for the present steady, conservative, linear case, since $\mathbf{F} = (0, -\rho_0 \overline{v'u'}, -\rho_0 \overline{w'u'})$ here [cf. Eq. (3.5.3)], and depends only on $z$.

As mentioned above, the small-scale gravity waves observed in the middle atmosphere tend to have vertical wavelengths less than about 15 km, so that $4H^2m^2 \geq 34$ if $H = 7$ km, and thus $m^2 \gg 1/4H^2$. It is therefore reasonable to neglect $1/4H^2$ compared with $m^2$ in Eq. (4.6.4); this is equivalent to making the "Boussinesq approximation," and gives $\omega^2 = N^2(k^2 + l^2)/m^2$. The solution with positive vertical group velocity $c_g^{(z)} \equiv \partial\omega/\partial m$ is

$$\omega = -N(k^2 + l^2)^{1/2}/m. \tag{4.6.5}$$

Numerous other properties of internal gravity waves are given in standard texts. In particular, the frequency $\omega$ is always smaller in magnitude than the buoyancy frequency $N$; indeed, under the hydrostatic approximation of Eq. (3.1.3c), $|\omega| \ll N$, as shown for example by Gill (1982, Section 6.14), and thus the period is much greater than $2\pi N^{-1}$ ($\approx$5 min in the middle atmosphere). The same inequality implies that the horizontal wavelength $2\pi(k^2 + l^2)^{-1/2}$ must be much larger than the vertical wavelength $2\pi|m|^{-1}$, by Eq. (4.6.5). Another interesting property is that if $i/2H$ is neglected in Eq. (4.6.3c)—a fair approximation for waves of vertical wavelength less than 15 km, for which $2H|m| \geq 5.8$—then Eqs. (4.6.3) and (4.6.5) give $(\hat{u}, \hat{v}, \hat{w}) \cdot (k, l, m) \approx 0$, so that the velocity $(u', v', w')$ is perpendicular to the wave vector $\mathbf{k} \equiv (k, l, m)$ and thus lies in planes of constant phase, $kx + ly + mz =$ constant. In this case parcel orbits are straight lines, also perpendicular to the wave vector.

It is often convenient to choose the horizontal axes so that $\mathbf{k} = (k, 0, m)$ and $l = 0$: this is possible since no preferred horizontal direction is imposed by the motionless basic state considered here. Then $\hat{v} = 0$ by Eq. (4.6.3b), and Eq. (4.6.5) becomes

$$\omega = -Nk/m, \tag{4.6.5'}$$

given the convention $k > 0$, as before. The vector group velocity is then

$$\mathbf{c}_g = \left(\frac{\partial\omega}{\partial k}, 0, \frac{\partial\omega}{\partial m}\right) = \frac{N}{m^2}(-m, 0, k), \tag{4.6.6}$$

and the tangent of the angle it makes with the horizontal has magnitude

$$|c_g^{(z)}/c_g^{(x)}| = |k/m| = |\omega/N|.$$

The foregoing theory can be extended to allow for a basic flow $[\bar{u}(z), \bar{v}(z), 0]$ and buoyancy frequency $N(z)$ that vary with height (although in this case one cannot generally chooose axes such that $l = 0$). When these quantities vary only on height scales much greater than a vertical wavelength, *WKBJ* methods analogous to those of Appendix 4A and Section 4.5.4 can be used, and ray-tracing can be carried out. Once again critical levels, at which $\omega = k\bar{u} + l\bar{v}$, need special attention.

### 4.6.2 *A Simple Model of Breaking Gravity Waves*

Owing to the presence of the $e^{z/2H}$ factor, proportional to $\rho_0^{-1/2}$, in Eq. (4.6.2), the linear, nondissipative theory of Section 4.6.1 predicts velocity and geopotential disturbances that grow with altitude; at some height the nonlinear terms that have been neglected will become important, and the linear theory will break down.

A physical picture of this breakdown can be obtained by considering a set of material surfaces at various levels, which are undulating as an internal gravity wave propagates vertically through them; Fig. 4.17 is a schematic diagram of this situation. In the lower mesosphere, say, the material surface (a) has a gentle sinusoidal variation, as predicted by linear theory. For gravity waves of period much less than a day the effects of radiative relaxation are small, and in the absence of other diabatic processes we can use an isentrope (a surface of constant $\theta$) as the material surface (a). In the middle mesosphere the material surface (b) is also sinusoidal, but of larger amplitude than (a); linear theory still holds, and (b) can also be taken as an isentrope. In the upper mesosphere, however, nonlinear effects become important, leading to the rapid and irreversible deformation of material contours such as (c), followed by turbulence, small-scale mixing,

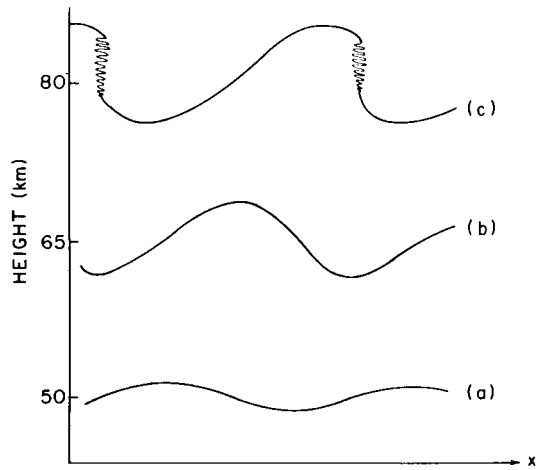


**Fig. 4.17.** Schematic diagram illustrating the breaking of vertically propagating internal gravity waves in the mesosphere. The curves labeled (a), (b), and (c) denote material surfaces. At the level of (a) and (b) the linear nondissipative theory of Section 4.6.1 is approximately valid. At the level of (c) nonlinear effects are important, with irreversible deformation of previously wavy material surfaces, and turbulence near the wave crests, presumably followed by small-scale mixing and dissipation.

and dissipation. Isentropes are no longer material surfaces, owing to the excitation of diabatic effects.

The process described here is known as *gravity-wave breaking*, by analogy with the overturning and breaking of oceanic surface waves on a shelving beach. It also has points in common with the phenomenon of planetary-wave breaking, described in Section 5.2.3. It will tend to limit the $e^{z/2H}$ growth of gravity wave amplitudes with height, and this has important consequences for the large-scale flow in the middle atmosphere, as will be seen below.

A simple model of this breaking process was suggested by Lindzen (1981), who considered linearized disturbances to a basic zonal flow $\bar{u}(z)$, and used a *WKBJ* method to generalize the solutions of Eq. (4.6.2). He then defined the *breaking level*, $z_b$, to be that altitude at which the isentropes first become vertical, with $\partial\theta/\partial z = 0$, thus implying a loss of static stability and the onset of turbulence and mixing. From Eqs. (3.2.13) and (3.4.2c)

$$\theta_z = \bar{\theta}_z + \theta'_z = HR^{-1}e^{\kappa z/H}[N^2 + \Phi'_{zz} + \kappa H^{-1}\Phi'_z], \tag{4.6.7}$$

and since $\Phi'$, as calculated by linear theory, grows exponentially with $z$ [cf. Eq. (4.6.2)], we expect that $-(\Phi'_{zz} + \kappa H^{-1}\Phi'_z)$ will at a sufficient altitude become large enough to cancel $N^2$ at some values of $x$, $y$, and $t$, at the "crests" of the waves. At such points $\theta_z = 0$, and breaking occurs, in Lindzen's sense. This approach is not strictly self-consistent, since the linear solutions will break down before such a height is reached; nevertheless it should give a qualitative feel for the fully nonlinear behavior.

In the special case where $\bar{u} = 0$ we can use the linear theory of Section 4.6.1 to illustrate Lindzen's approach. We choose axes such that $l = 0$ and thus $v' = 0$, and suppose that $\Phi' = \Phi_0 \cos k(x - ct)$ at some lower level, which can be taken as $z = 0$ by suitable choice of $p_s$. Thus the solutions of Eq. (4.6.2) apply, subject to Eq. (4.6.3) with $l = 0$, $\hat{\Phi} = \Phi_0$ (real), and $\omega = ck$; in particular,

$$\Phi' = \Phi_0 e^{z/2H} \cos[k(x - ct) + mz]. \tag{4.6.8}$$

Assuming once more that vertical wavelengths are small enough to ensure that $|m| \gg 1/2H$, we have

$$\Phi'_{zz} + \kappa H^{-1}\Phi'_z \approx -m^2\Phi' = -m^2\Phi_0 e^{z/2H} \cos[k(x - ct) + mz].$$

The breaking level $z_b$ is defined by $\{\max|\Phi'_{zz} + \kappa H^{-1}\Phi'_z|\}_{z=z_b} = N^2$, and so

$$z_b \approx 2H \ln\left|\frac{N^2}{m^2\Phi_0}\right| = 2H \ln|c^2\Phi_0^{-1}| \tag{4.6.9}$$

by Eqs. (4.6.8) and (4.6.5′) with $c = \omega/k$. Note that $z_b$ depends on the phase speed $c$ and the initial geopotential amplitude $\Phi_0$ of the wave; it increases as $\Phi_0$ decreases because waves of small amplitude need to penetrate to

greater heights before they have grown enough to break than do waves of larger amplitude.

The next step is to describe what happens above the breaking level. The turbulence that presumably sets in leads to diffusion of heat and momentum, and a crude way of parameterizing this diffusion is to modify Eqs. (4.6.1a,d) thus:

$$u'_t + \Phi'_x = Ku'_{zz}, \qquad \Phi'_{zt} + N^2 w' = K\Phi'_{zzz}, \qquad z > z_b, \qquad (4.6.10a,b)$$

where $K$ is a constant diffusion coefficient; above $z_b$ the continuity equation, Eq. (4.6.1c), still holds. On seeking solutions of the form

$$\Phi' = e^{z/2H}\,\mathrm{Re}[\Phi_1 \exp i(kx + m_1 z - kct)]$$

above $z_b$, chosen to match Eq. (4.6.8) at $z_b$, we find

$$\omega + im_1^2 K = -Nk/m_1 \qquad (4.6.11)$$

by analogy with (4.6.5′), where the convention $k > 0$ is retained. Thus if $K$ is chosen so small that

$$m^2 K \ll |\omega|, \qquad (4.6.12)$$

it follows that

$$m_1 \approx -\frac{Nk}{\omega} + \frac{iKN^3k^3}{\omega^4} = m + \frac{iKN^3}{c^4 k}$$

and so

$$\Phi' = \Phi_0 \exp\left[\frac{z}{2H} - \frac{KN^3}{c^4 k}(z - z_b)\right] \cos[k(x - ct) + mz], \qquad z > z_b, \qquad (4.6.13)$$

to satisfy continuity with Eq. (4.6.8) at $z_b$. The extra exponential factor involving $K$ results from the postulated diffusive damping of the waves due to breaking. Lindzen hypothesizes that above $z_b$ the waves are *saturated*, or just on the verge of breaking; thus $\max|\Phi'_{zz} + \kappa H^{-1}\Phi'_z| = N^2$ for all $z \geq z_b$. Hence the diffusive decay must be such as to exactly balance the $e^{z/2H}$ growth, and $K$ must be chosen such that the coefficient of $z$ in the exponential term in Eq. (4.6.13) vanishes, that is,

$$K = c^4 k/2HN^3. \qquad (4.6.14)$$

Note that this implies

$$m^2 K = \frac{N^2 k^2}{\omega^2}\left(\frac{c^4 k}{2HN^3}\right) = \frac{c^2 k}{2HN} = \left|\frac{\omega}{2Hm}\right|$$

by Eq. (4.6.5′), and thus Eq. (4.6.12) is consistent with our previous assumption that $|m| \gg 1/2H$. Substitution of Eq. (4.6.14) into Eq. (4.6.13) gives

$$\Phi' = \Phi_0 e^{z_b/2H} \cos[k(x - ct) + mz] \qquad \text{for} \quad z \geq z_b, \tag{4.6.15a}$$

while Eqs. (4.6.10a,b) yield

$$(u', w') = (1, -k/m)c^{-1}\Phi_0 e^{z_b/2H} \cos[k(x - ct) + mz] \qquad \text{for} \quad z \geq z_b \tag{4.6.15b,c}$$

at leading order in the small parameter $m^2K/\omega$. Thus Lindzen's saturation hypothesis implies no further growth of wave amplitude above $z_b$: this is roughly consistent with observed gravity-wave amplitudes in the mesosphere. Note, incidentally, that $\max|u'| = |c|$ for $z \geq z_b$, from Eqs. (4.6.15b) and (4.6.9).

We now calculate the quantity

$$\bar{X}_1 \equiv -\rho_0^{-1}(\rho_0 \overline{u'w'})_z; \tag{4.6.16}$$

using Eqs. (4.6.15b,c), (4.6.9), (4.6.5′), and (4.6.14) it follows that

$$\bar{X}_1 = c^3 k/2NH = \frac{N^2 K}{c} \qquad \text{for} \quad z > z_b, \tag{4.6.17}$$

which is a nonzero constant in general. Thus if $c > 0$ there is a zonal-mean vertical wave momentum flux convergence or Eliassen-Palm flux divergence above the breaking level (and vice versa if $c < 0$), and this implies a contribution to the wave-induced forcing of the zonal-mean flow. Lindzen also postulates that the momentum and heat diffusion represented by $K$ acts on the zonal-mean flow, as well as on the gravity waves.

As mentioned above, Lindzen's method is more general than that given here, in that it includes a slowly varying mean flow $[\bar{u}(z), 0, 0]$ and nonzero meridional wave number $l$. The generalization of Eq. (4.6.17) is

$$\bar{X}_1 = \frac{(c - \bar{u})^3 k}{2N}\left[\frac{1}{H} + \frac{3\, d\bar{u}/dz}{c - \bar{u}}\right] = \frac{N^2 K}{c - \bar{u}} \tag{4.6.18a,b}$$

when $l = 0$ but $\bar{u} \neq 0$. On substituting typical wave parameters, such as those given at the beginning of Section 4.6, into these formulas, it is found that Lindzen's parameterization of the possible frictional effects due to breaking gravity waves implies a strong forcing of the zonal-mean circulation of the upper mesosphere, in accordance with observations that indicate that $\bar{X}_1$ may be on the order of several tens of meters per second per day (see Fig. 4.18). This topic will be discussed further in Sections 7.3 and 8.5.

It is also possible to allow for the radiative damping of gravity waves in the above theory. Since damping tends to decrease the amplitude of the

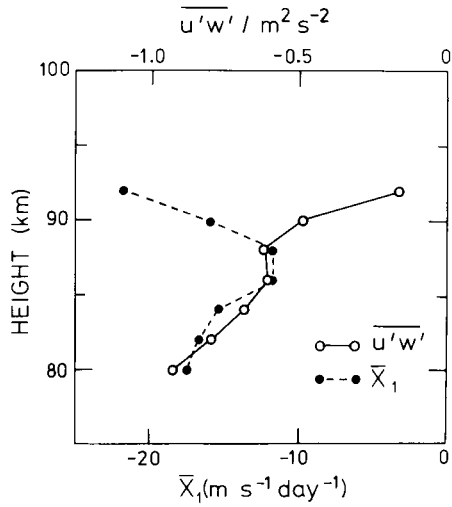


**Fig. 4.18.** Height profiles of $\overline{u'w'}$ and $\bar{X}_1$, in the upper mesosphere, derived from double-beam radar measurements in May 1981. [After Vincent and Reid (1983).]

upward-propagating waves, the breaking level tends to be raised; indeed, waves of sufficiently small intrinsic phase speed may not break at all. However, if they do break, the radiative damping has little effect on the resulting values of $\bar{X}_1$.

It has been emphasized that Lindzen's model is highly simplified, being essentially based on a linear theory of monochromatic gravity waves. Much more observational and theoretical work needs to be done to investigate the validity of the model and to understand the detailed nonlinear dynamics of a complex spectrum of breaking gravity waves (for which a "breaking amplitude" is more appropriate than a "breaking level") and their effects on the mean flow.

### *4.6.3 Inertio-Gravity Waves*

On somewhat larger space and time scales (horizontal wavelengths ~1000 km and periods of several hours) than those considered in Section 4.6.1, gravity waves will be influenced by the rotation of the earth, and the theory given there will need modification. As a simple example that avoids the complexity of the spherical geometry used in Section 4.2, we consider small disturbances to a state of rest on an "$f$-plane," in which the Coriolis

parameter $f$ is taken as constant. Then Eqs. (4.6.1) are replaced by

$$u'_t - fv' + \Phi'_x = 0, \tag{4.6.19a}$$

$$v'_t + fu' + \Phi'_y = 0, \tag{4.6.19b}$$

$$u'_x + v'_y + \rho_0^{-1}(\rho_0 w')_z = 0, \tag{4.6.19c}$$

$$\Phi'_{zt} + N^2 w' = 0. \tag{4.6.19d}$$

Taking $N$ constant again, and substituting

$$(u', v', w', \Phi') = e^{z/2H}\,\mathrm{Re}[(\hat{u}, \hat{v}, \hat{w}, \hat{\Phi})\exp i(kx + ly + mz - \omega t)] \tag{4.6.20}$$

once more, we obtain the equations

$$\hat{u} = (\omega^2 - f^2)^{-1}(\omega k + ilf)\hat{\Phi}, \tag{4.6.21a}$$

$$\hat{v} = (\omega^2 - f^2)^{-1}(\omega l - ikf)\hat{\Phi}, \tag{4.6.21b}$$

$$\hat{w} = -\frac{\omega}{N^2}\left(m - \frac{i}{2H}\right)\hat{\Phi}, \tag{4.6.21c}$$

and the dispersion relation

$$\omega^2 = f^2 + \frac{N^2(k^2 + l^2)}{m^2 + 1/4H^2}. \tag{4.6.22}$$

These clearly reduce to Eqs. (4.6.3) and (4.6.4) when $f = 0$.

Some important properties of inertio-gravity waves follow from these results. Note first from Eq. (4.6.22) that the existence of propagating waves, with $k$, $l$, $m$ all real, requires that

$$|f| \leqslant |\omega| \ll N, \tag{4.6.23}$$

where the right-hand inequality results from the hydrostatic approximation, as in Section 4.6.1. The left-hand inequality shows that the frequency of inertio-gravity waves is greater than the Coriolis parameter; this is a qualitative explanation of the confinement of propagating diurnal tides ($|\omega| = \Omega$) to the region where $|f| \equiv 2\Omega|\sin\phi| \leqslant \Omega$, that is, equatorward of 30° latitude (see Section 4.3.3). On the other hand, since the present analysis does not take account of the global variation of $f$, a detailed comparison of Eq. (4.6.22) with the dispersion curves plotted in Figs. 4.2a,b is difficult, except in the "nonrotating" limit $\gamma^{-1/2} \to \infty$ mentioned in Section 4.6.1. (A better comparison between the full spherical-geometry theory and a simpler analysis occurs as $\gamma^{-1/2} \to 0$ and the modes become equatorially trapped: see Section 4.7.)

From Eq. (4.6.22) we can obtain the group velocity; we choose axes such that $l = 0$ as before, and use the approximation $m^2 \gg 1/4H^2$. Then

$$\omega = \pm(f^2 + N^2k^2/m^2)^{1/2} \tag{4.6.24}$$

and

$$\mathbf{c}_g = \frac{N^2k}{m^3\omega}(m, 0, -k); \tag{4.6.25}$$

moreover,

$$|c_g^{(z)}/c_g^{(x)}| = |k/m| = (\omega^2 - f^2)^{1/2}/N, \tag{4.6.26}$$

and this is generally smaller than for pure internal gravity waves [cf. Eq. (4.6.6)] since $k$ is smaller, while $m$ is about the same. Thus inertio-gravity waves will tend to propagate more horizontally than do pure internal waves, other things being equal.

One way of identifying the sign of $c_g^{(z)}$ from measurements of an inertio-gravity wave is to determine the sense of rotation of the horizontal velocity vector $(u', v', 0)$ with height. Taking $l = 0$ in Eqs. (4.6.21a,b) and setting $\hat{u}$ real (by a suitable choice of the time origin, say) we obtain

$$\tan \xi \equiv v'/u' = f\omega^{-1} \tan(kx + mz - \omega t),$$

where $\xi$ is the angle between $(u', v', 0)$ and the positive $x$ axis. Then, differentiating with respect to $z$,

$$\sec^2 \xi \frac{\partial \xi}{\partial z} = f\omega^{-1}m \sec^2(kx + mz - \omega t)$$

so that $\partial\xi/\partial z$ has the same sign as $f\omega^{-1}m$; by Eq. (4.6.25) it follows that

$$\operatorname{sgn}(\partial\xi/\partial z) = -\operatorname{sgn}(fc_g^{(z)}).$$

Thus the horizontal velocity vector rotates anticyclonically with height (clockwise in the northern hemisphere, anticlockwise in the southern hemisphere) for upward-propagating waves ($c_g^{(z)} > 0$), and cyclonically for downward-propagating waves ($c_g^{(z)} < 0$). [The same result can be proved when $l \neq 0$ by defining $\xi$ as the angle between $(u', v', 0)$ and the horizontal wave vector $(k, l, 0)$.] In practice, this method is usually applied to measurements of inertio-gravity-wave spectra, rather than single waves.

The orbits of fluid parcels in inertio-gravity waves can be calculated by the methods of Section 4.5.3. In particular, when $|m| \gg 1/2H$ parcels move anticyclonically in ellipses in planes perpendicular to the wave vector $(k, l, m)$: see Fig. 4.19.

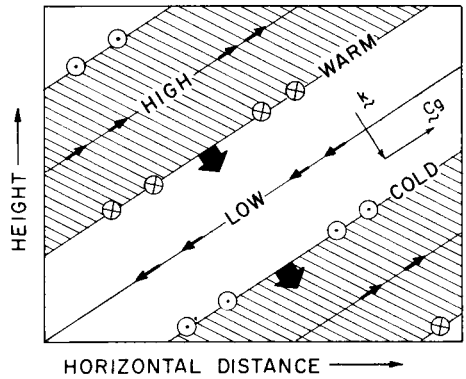


**Fig. 4.19.** Vertical section in a plane containing the wave vector **k** showing the phase relationships between velocity, geopotential, and temperature ($\propto \Phi'_z$) fluctuations in an upward-propagating inertio-gravity wave, with $|m| \gg 1/2H$, $m < 0$, $\omega > 0$ in the northern hemisphere ($f > 0$). The thin sloping lines denote the surfaces of constant phase (perpendicular to the wave vector) and thick arrows show the direction of phase propagation. The wave vector and group velocity are also shown. The same diagram applies to the pure internal gravity waves of Section 4.6.1 and the Kelvin waves of Section 4.7.1 if the arrows indicating velocity components into and out of the page are omitted, and if "horizontal" is taken to mean "eastward" in the Kelvin wave case.

## 4.7 Equatorial Waves

It has been known for many years that large-scale, equatorially confined wave motions propagate vertically and zonally through the middle atmosphere. These waves have periods of a few days and are of planetary scale in the zonal direction, but are trapped within about 15° north and south of the equator. The earliest observations of such waves were from radiosondes in the lower stratosphere, and more recently rocketsondes and satellites have detected them in the upper stratosphere and mesosphere as well; these observations will be discussed in Section 4.7.5. Waves of this kind are particularly significant for the dynamics of the middle atmosphere, since they are believed to play a central role in forcing the equatorial quasi-biennial oscillation (QBO) and semiannual oscillation (SAO): see Chapter 8.

A natural starting point for a theory of these equatorial waves is the fact, mentioned in Section 4.2, that as $\gamma^{-1/2} \equiv (gh)^{1/2}/2\Omega a \to 0$, all the Hough modes become confined near the equator; this is evident for example in Figs. 7–13 of Longuet-Higgins (1968). The latitudinal confinement suggests that a beta-plane approximation may be satisfactory for studying these modes, and we shall adopt such an approach in this section, so as to avoid the complexities of spherical geometry. The beta-plane will be centered at

the equator so that $f_0 = 0$ and $f = \beta y$, where $\beta = 2\Omega a^{-1}$ [cf. Eq. (3.2.1f)] and $y$ is distance north of the equator. The vanishing of $f$ at the equator suggests that the quasi-geostrophic equations will not generally be valid: for example, the condition of Eq. (3.2.8a) on the Rossby number will usually be violated. We therefore work with the primitive equations, which, when linearized about a basic zonal flow $\bar{u}(y, z)$, become

$$\bar{D}u' + (\bar{u}_y - \beta y)v' + \bar{u}_z w' + \Phi'_x = X', \tag{4.7.1a}$$

$$\bar{D}v' + \beta y u' + \Phi'_y = Y', \tag{4.7.1b}$$

$$\Phi'_z = H^{-1}R\theta' e^{-\kappa z/H}, \tag{4.7.1c}$$

$$u'_x + v'_y + \rho_0^{-1}(\rho_0 w')_z = 0, \tag{4.7.1d}$$

$$\bar{D}\theta' + \bar{\theta}_y v' + \bar{\theta}_z w' = Q', \tag{4.7.1e}$$

where $\bar{D} = \partial/\partial t + \bar{u}\,\partial/\partial x$. These equations follow from Eqs. (3.4.2) on setting $f = \beta y$, $\cos\phi = 1$, $\tan\phi = 0$, and using Cartesian coordinates $(x, y)$, where the $x$ axis points eastward along the equator. The thermal wind equation for the basic flow,

$$\beta y \bar{u}_z = -H^{-1}R\bar{\theta}_y e^{-\kappa z/H}, \tag{4.7.2}$$

follows similarly from Eq. (3.4.1c).

Aspects of the roles of the frictional and diabatic terms $X'$, $Y'$, and $Q'$ in forcing and dissipating equatorial waves will be discussed in Sections 4.7.3 and 4.7.4. However, the simplest way of deriving the basic theoretical equatorial wave structures is to ignore such nonconservative processes for the moment by setting $X' = Y' = Q' = 0$, and also to neglect the complicating effects of the basic wind shear by setting $\bar{u} = 0$ and thus $\bar{\theta}_y = 0$, by Eq. (4.7.2). (The effects of a constant nonzero $\bar{u}$ will be mentioned later.) The disturbances then satisfy

$$u'_t - \beta y v' + \Phi'_x = 0, \tag{4.7.3a}$$

$$v'_t + \beta y u' + \Phi'_y = 0, \tag{4.7.3b}$$

$$u'_x + v'_y + \rho_0^{-1}(\rho_0 w')_z = 0, \tag{4.7.3c}$$

$$\Phi'_{zt} + N^2 w' = 0, \tag{4.7.3d}$$

where Eqs. (4.7.1c,e) have been combined to give Eq. (4.7.3d), as in Eq. (4.2.1), and $N^2(z) = H^{-1}R\bar{\theta}_z e^{-\kappa z/H}$ as before. For simplicity we set $N =$ constant, and then seek solutions in the form

$$(u', v', w', \Phi') = e^{z/2H}\,\mathrm{Re}\{[\hat{u}(y), \hat{v}(y), \hat{w}(y), \hat{\Phi}(y)]\exp i(kx + mz - \omega t)\}. \tag{4.7.4}$$

We obtain

$$\hat{w} = -\frac{\omega}{N^2}\left(m - \frac{i}{2H}\right)\hat{\Phi} \tag{4.7.5}$$

from Eq. (4.7.3d) and

$$-i\omega\hat{u} - \beta y\hat{u} + ik\hat{\Phi} = 0, \tag{4.7.6a}$$

$$-i\omega\hat{v} + \beta y\hat{u} + \hat{\Phi}_y = 0, \tag{4.7.6b}$$

$$ik\hat{u} + \hat{v}_y - i\omega m^2 N^{-2}\hat{\Phi} = 0, \tag{4.7.6c}$$

from Eqs. (4.6.3a,b,c) and (4.7.5). In Eq. (4.7.6c) a factor $m^2 + (1/4H^2)$ [which by Eq. (4.5.19) equals the $N^2/gh$ of classical tidal theory] has been replaced by $m^2$. This "Boussinesq" approximation is a reasonable one for many of the observed equatorial waves that, like the gravity waves of Section 4.6, have vertical wavelengths less than about 15 km, so that $4H^2m^2 \geqslant 34$. The approximation is more doubtful for the "fast" Kelvin waves observed in the upper stratosphere, which may have vertical wavelengths of about 40 km; however, the theory is easily reworked with the inclusion of the $1/4H^2$ term.

It will be observed that two $y$ derivatives appear in Eqs. (4.7.6): calculation of the latitudinal wave structures therefore generally involves the solution of a second-order ordinary differential equation in $y$. This equation, Eq. (4.7.11), is discussed in Section 4.7.2; we first consider a special case in which only a first-order ordinary differential equation need be solved.

### *4.7.1 The Kelvin Wave*

Among the equatorially trapped waves that are observed in the stratosphere and mesosphere (see Section 4.7.5) is a class of modes with small meridional wind component $v'$. As a first attempt to model these waves we look for solutions to Eqs. (4.7.6) in which $\hat{v}$ is identically zero; thus $\hat{u}$ and $\hat{\Phi}$ must satisfy

$$-\omega\hat{u} + k\hat{\Phi} = 0, \qquad \beta y\hat{u} + \hat{\Phi}_y = 0, \qquad k\hat{u} - \omega m^2 N^{-2}\hat{\Phi} = 0. \tag{4.7.7a,b,c}$$

If $\hat{u}$ and $\hat{\Phi}$ do not vanish, Eqs. (4.7.7a,c) immediately give $\omega = \pm Nkm^{-1}$, with vertical group velocity $c_g^{(z)} \equiv \partial\omega/\partial m = \mp Nkm^{-2}$. Anticipating that the root with positive $c_g^{(z)}$ will be the relevant one for the middle atmosphere, corresponding to a wave that propagates upward from the troposphere, we therefore have

$$\omega = -Nk/m \tag{4.7.8a}$$

and

$$c_g^{(z)} = Nk/m^2 = \omega^2/Nk \tag{4.7.8b}$$

if $k$ is chosen positive, by our usual convention. The dispersion relation, Eq. (4.7.8a), is identical to that for pure internal gravity waves with $l = 0$; see Eq. (4.6.5′).

The meridional structure of this wave solution can be found by eliminating $\hat{u}$ from Eqs. (4.7.7a,b) to obtain the first-order ordinary differential equation (ODE)

$$\hat{\Phi}_y + k\beta\omega^{-1}y\hat{\Phi} = 0,$$

which has the solution

$$\hat{\Phi}(y) = \hat{\Phi}_0 \exp(-\beta k y^2/2\omega), \tag{4.7.9}$$

where $\hat{\Phi}_0$ is a constant. If $\hat{\Phi}$ and $\hat{u}$ are to be bounded far from the equator, where $|y|$ becomes large, it is necessary that the coefficient of $y^2$ in the exponent in Eq. (4.7.9) be negative, and thus that $c = \omega/k$ be positive: this mode therefore has an eastward zonal phase speed and, by Eq. (4.7.8a), a negative value of $m$. The surfaces of constant phase $(kx + mz - \omega t)$ thus tilt eastward with height and move downward with time, as indicated in Fig. 4.19; a plan view of the meridional structure is shown in Fig. 4.20. The wave solution is called an *equatorial Kelvin wave*; its structure in the $xz$ plane is analogous to that of an internal gravity wave, and the $y$ variation given by Eq. (4.7.9) allows geostrophic balance to hold (exceptionally) right up to the equator.

A similar analysis can be performed in the case when $\bar{u}$ is constant and nonzero: the same formulas hold except that the absolute frequency $\omega$ is replaced by the intrinsic, or Doppler-shifted, frequency

$$\omega^+ \equiv \omega - k\bar{u}. \tag{4.7.10}$$

Use of this crude allowance for a basic zonal wind gives quite good agreement between theory and observation, as will be mentioned in Section 4.7.5. In particular $\omega^+/k > 0$, so that the absolute phase speed $\omega/k$ must be eastward with respect to the basic flow, and this is in accord with observations of Kelvin waves.

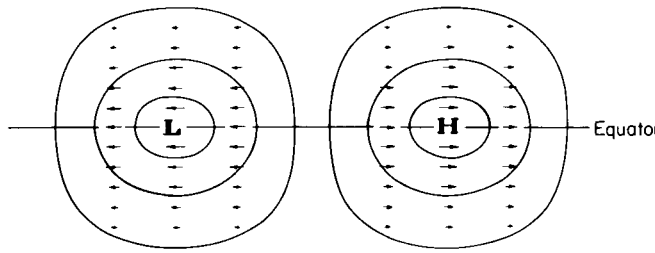


**Fig. 4.20.** Schematic illustration of geopotential and horizontal wind fluctuations for the Kelvin wave. [Adapted from Matsuno (1966).]

### 4.7.2 *Modes with Nonzero Meridional Velocity*

We now consider the case $\hat{v} \not\equiv 0$, and return to Eq. (4.7.6). On eliminating $\hat{u}$ and $\hat{\Phi}$ from Eqs. (4.7.6a,c) and substituting in Eq. (4.7.6b), we obtain

$$\left[\frac{d^2}{dy^2} + \left(\frac{m^2\omega^2}{N^2} - k^2 - \frac{k\beta}{\omega}\right) - \frac{\beta^2 m^2}{N^2} y^2\right]\hat{v} = 0, \tag{4.7.11}$$

provided that

$$m^2\omega^2 \neq N^2k^2. \tag{4.7.12}$$

The substitutions

$$\eta \equiv \left(\frac{\beta|m|}{N}\right)^{1/2} y, \qquad M \equiv \frac{N}{\beta|m|}\left(\frac{m^2\omega^2}{N^2} - k^2 - \frac{k\beta}{\omega}\right), \tag{4.7.13a,b}$$

where $|m|$ is assumed nonzero, allow Eq. (4.7.11) to be reduced to the dimensionless form

$$\left(\frac{d^2}{d\eta^2} + M - \eta^2\right)\hat{v} = 0, \tag{4.7.13c}$$

which also arises in the theory of the quantum harmonic oscillator and has the solutions

$$\hat{v} = \hat{v}_0 e^{-(1/2)\eta^2} H_n(\eta)$$

if $M = 2n + 1$, where $n$ is a nonnegative integer, the $H_n$ are the Hermite polynomials ($H_0 = 1$, $H_1 = 2\eta$, $H_2 = 4\eta^2 - 2$, etc.) and $\hat{v}_0$ is constant. Thus Eq. (4.7.11) has solutions

$$\hat{v} = \hat{v}_0 \exp(-\beta|m|y^2/2N) H_n[(\beta|m|N^{-1})^{1/2} y], \tag{4.7.14a}$$

provided that

$$\frac{m^2\omega^2}{N^2} - k^2 - \frac{\beta k}{\omega} = (2n + 1)\frac{\beta|m|}{N}. \tag{4.7.15}$$

Using Eqs. (4.7.6a,c) and the identities $dH_n/d\eta = 2nH_{n-1}$, $H_{n+1} = 2\eta H_n - 2nH_{n-1}$, it can be shown that

$$\hat{u} = i\hat{v}_0(\beta|m|N)^{1/2}\left[\frac{\frac{1}{2}H_{n+1}(\eta)}{|m|\omega - Nk} + \frac{nH_{n-1}(\eta)}{|m|\omega + Nk}\right]e^{-(1/2)\eta^2}, \tag{4.7.14b}$$

$$\hat{\Phi} = i\hat{v}_0\left(\frac{\beta N^3}{|m|}\right)^{1/2}\left[\frac{\frac{1}{2}H_{n+1}(\eta)}{|m|\omega - Nk} - \frac{nH_{n-1}(\eta)}{|m|\omega + Nk}\right]e^{-(1/2)\eta^2}, \tag{4.7.14c}$$

and $\hat{w}$ follows from Eqs. (4.7.5) and (4.7.14c). These solutions are trapped near the equator, with a latitudinal decay scale of order $(2N/\beta|m|)^{1/2}$; for a vertical wavelength of 10 km, this is approximately 1660 km or 15 degrees of latitude. [The same scale $(2N/\beta|m|)^{1/2}$ applies for Kelvin waves, as can be seen from Eqs. (4.7.9) and (4.7.8a) and the fact that $m < 0$ in this case.] The "turning point," at which $\hat{v}$ changes from oscillatory behavior to exponential decay, is seen from Eq. (4.7.13c) to occur at $\eta = \pm M^{1/2}$, that is, $y = \pm[(2n+1)N/\beta|m|]^{1/2}$. Note that the solutions, Eqs. (4.7.9) and (4.7.14c), are the equatorial beta-plane analogs of the Hough functions of Section 4.2 in the limit $\gamma^{-1/2} \to 0$.

The gravest of the modes with nonzero $\hat{v}$ is of particularly simple form: setting $n = 0$ in Eq. (4.7.15) we obtain

$$(|m|\omega - Nk)(|m|\omega + Nk) = \beta\omega^{-1}N(|m|\omega + Nk);$$

but by Eq. (4.7.12), $|m|\omega + Nk \neq 0$, so this factor can be canceled to give

$$|m| = \frac{N}{\omega^2}(\beta + \omega k) \tag{4.7.16}$$

as the dispersion relation for the $n = 0$ mode; since $|m|$ is positive it follows that

$$c \equiv \omega/k > -\beta/k^2. \tag{4.7.17}$$

Equation (4.7.16) can be written $m = \pm N\omega^{-2}(\beta + \omega k)$, so that

$$c_g^{(z)} = \frac{\partial\omega}{\partial m} = \left(\frac{\partial m}{\partial\omega}\right)^{-1} = \frac{\mp\omega^3}{N(2\beta + \omega k)}. \tag{4.7.18}$$

The denominator of the last term in Eq. (4.7.18) is positive, by Eq. (4.7.17), and thus the choice of sign for upward group velocity $c_g^{(z)}$ depends on the sign of $\omega$. If $-\beta/k < \omega < 0$ the upper sign applies, while if $\omega > 0$ the lower sign applies; the dispersion relation [Eq. (4.7.16)] therefore becomes

$$m = -\text{sgn}(\omega)\frac{N}{\omega^2}(\beta + \omega k). \tag{4.7.16'}$$

Since $H_0 = 1$, the solution is found to be

$$(\hat{u}, \hat{v}, \hat{\Phi}) = \hat{v}_0\left(\frac{i|m|\omega y}{N}, 1, i\omega y\right)\exp\left(\frac{-\beta|m|y^2}{2N}\right); \tag{4.7.19}$$

this solution is called the *Rossby-gravity wave*; its structures in the $xz$ and $xy$ planes are illustrated in Figs. 4.21 and 4.22. It approximately corresponds to an observed stratospheric wave disturbance if allowance is again made for a basic flow $\bar{u}$ by replacing $\omega$ by $\omega^+ = \omega - k\bar{u}$. The observed wave has

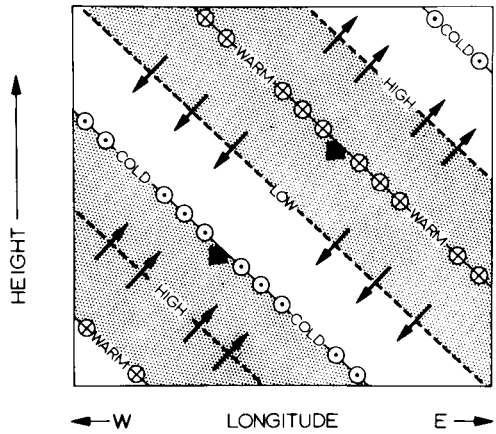


**Fig. 4.21.** Longitude–height section at a latitude north of the equator, showing geopotential, temperature, and wind fluctuations in the Rossby-gravity wave of westward phase speed $(-\beta/k < \omega < 0)$ when $|m| \gg 1/2H$. Northward winds are indicated by arrows into the page and southward winds by arrows out of the page. Thick arrows indicate direction of phase propagation. [After Holton (1975). American Meteorological Society.]

a westward phase speed with respect to the mean flow, so that $\omega^+/k < 0$: see Section 4.7.5.

The equatorial modes for $n \geq 1$ have more complex meridional structure than the Kelvin and Rossby-gravity modes. Their dispersion relation, Eq. (4.7.15), is a quadratic in $|m|$ if $k(>0)$, $\omega$ and $n$ are given, and the solutions fall into two categories. First, there is a set of high-frequency *equatorial inertio-gravity waves*, with dispersion relations

$$m = -\mathrm{sgn}(\omega) N\beta\omega^{-2}\{(n+\tfrac{1}{2}) + [(n+\tfrac{1}{2})^2 + \omega k\beta^{-1}(1+\omega k\beta^{-1})]^{1/2}\}, \quad (4.7.20)$$

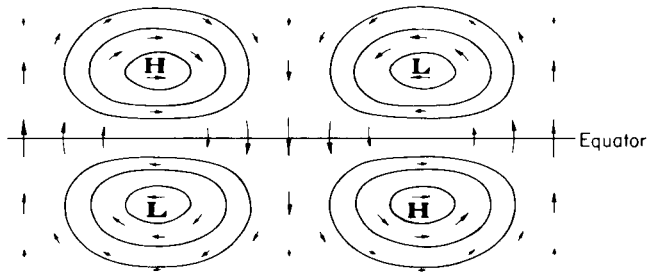


**Fig. 4.22.** Schematic illustration of geopotential and horizonal wind fluctuations for the Rossby-gravity wave of westward phase speed. [Adapted from Matsuno (1966).]

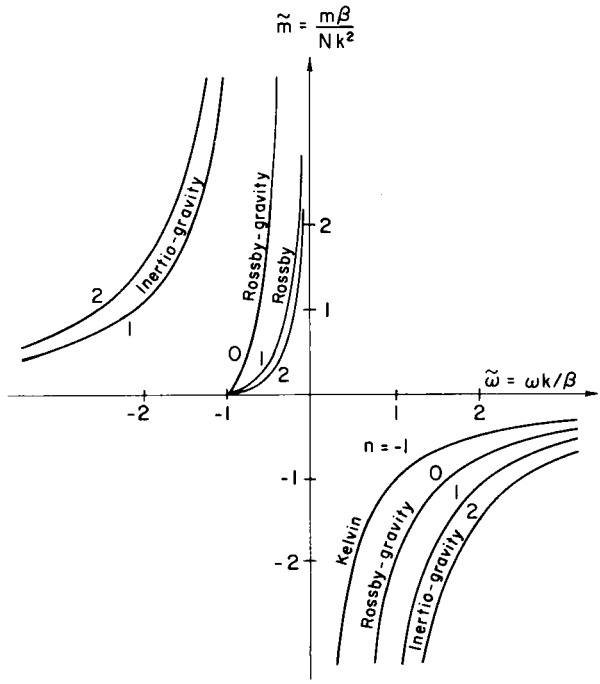


**Fig. 4.23.** Dispersion curves for upward-propagating equatorial waves. See text for details.

which occur for all values of $\omega$. Second, there is a set of low-frequency *equatorial Rossby waves*, with dispersion relations

$$m = N\beta\omega^{-2}\{(n+\tfrac{1}{2}) - [(n+\tfrac{1}{2})^2 + \omega k\beta^{-1}(1+\omega k\beta^{-1})]^{1/2}\}, \qquad (4.7.21)$$

which only occur for $-\beta k^{-2} < c \equiv \omega/k < 0$. (This condition on the phase speed also happens to be a corollary of the Charney-Drazin condition [Eq. (4.5.15)] for midlatitude Rossby waves when $\bar{u} = 0$, since $\bar{u}_c < \beta k^{-2}$.) In Eqs. (4.7.20) and (4.7.21) we have given only the solutions corresponding to an upward group velocity. Dispersion curves are presented in Fig. 4.23 in terms of the dimensionless parameters $\tilde{m} \equiv m\beta/Nk^2$ and $\tilde{\omega} \equiv \omega k/\beta$, for several values of $n \geq 1$. Also plotted are the dispersion curves for the upward-propagating Rossby-gravity wave ($n = 0$) with the dispersion relation of Eq. (4.7.16′) and Kelvin wave (often designated by the index $n = -1$) with the dispersion relation of Eq. (4.7.8a).[3] Other ways of plotting the

[3] The index $n$, which has been used here to distinguish the various equatorial wave modes, corresponds to $n_E$ appearing at the left-hand end of the curves in Figs. 4.2a,b.

equatorial-wave dispersion relations are given for example by Gill (1982), Figs. 11.1 ($\omega$ versus $k$ at fixed $m$) and 11.8 ($m$ versus $k$ at fixed $\omega$).

### 4.7.3 *The Forcing of Equatorial Waves*

The upward-propagating equatorial waves that are observed in the middle atmosphere are generally thought to be forced by geographically confined time variations in the large-scale cumulus convective heating in the equatorial troposphere. A simple way of modeling this forcing is to include a heating term $J'(x, y, z, t)$ in a lower region $0 \leq z < z_1$ representing the troposphere, but to retain $J' = 0$ for $z \geq z_1$. The theory given above relates to the latter region, provided $N$ is still assumed to be constant there and the approximation $m^2 \gg 1/4H^2$ still holds.

The temporal variability in $J'$ is approximated by a single standing oscillation of the form

$$J' = 2F(y)G(z) \cos kx \cos \omega t \tag{4.7.22a}$$

$$= F(y)G(z)[\cos(kx - \omega t) + \cos(kx + \omega t)], \tag{4.7.22b}$$

where $F(y)$ is confined near to the equator and $G(z)$, the vertical distribution of heating, is specified to fit the mean profile observed for tropical cloud clusters (Fig. 4.24); it vanishes for $z \geq z_1$. Equation (4.7.22b) shows that the standing oscillation can be represented as a superposition of eastward and westward moving forcing terms. If $\kappa J'/H$ is now included on the right of Eq. (4.7.3d), Eqs. (4.7.3) are analogous to Eqs. (4.2.1) of classical tidal theory, except that the equatorial beta-plane is used, rather than spherical geometry. By linearity, the responses to the eastward and westward traveling forcing in Eq. (4.7.22b) can be found separately, and then summed. The method is similar to that of tidal theory: for the specified $k$ and $\omega$, the

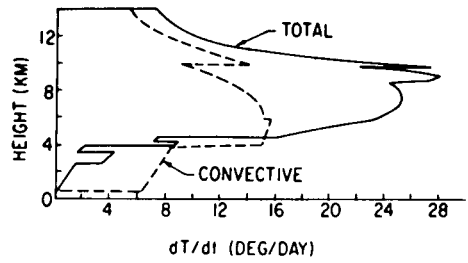


**Fig. 4.24.** Observed vertical profile of total large-scale diabatic heating by mature cloud clusters in the tropical troposphere (solid curve). Heating by convective towers alone (dashed curve) is shown for comparison. [After Houze (1982).]

relevant modes and their vertical wave numbers $m$ can be read off from a diagram like Fig. 4.23. The function $F(y)$ is then expanded in the geopotential eigenfunctions associated with these modes; since the latter are limiting cases of the Hough functions, they form a complete set. The response, say in $\hat{w}$, is similarly summed, and the $z$-dependent amplitudes of the eigenfunctions found by solving a vertical structure equation like Eq. (4.3.4), but with $N^2/gh_n - (1/4H^2)$ replaced by $m^2$ for the relevant mode. In detailed calculations, the non-Boussinesq version of the theory might be needed if values of $m^2$ arise that are not much larger than $1/4H^2$.

A simple model of this form has been used by Chang (1976) to explain the observed distribution of Kelvin waves. In general, however, a more detailed calculation is probably needed, to examine the mechanism of the excitation of equatorial waves. For example, Holton (1972) used a model involving a longitudinally localized heat source and a basic zonal shear flow $\bar{u}(z)$ to account for the observed Rossby-gravity waves. Further details of these studies are given in Section 4.7.5. Strong support for the hypothesis that both Kelvin and Rossby-gravity waves are indeed forced by tropical convective heating has been provided by Hayashi and Golder (1978) by means of controlled experiments with a sophisticated nonlinear general circulation model.

### *4.7.4 WKBJ Theory of Dissipating Equatorial Waves in a Shear Flow*

As mentioned above, the theory given in Sections 4.7.1 and 4.7.2 immediately extends to the case in which a constant basic zonal flow is present but dissipation is neglected. However, the influence of basic shear, particularly vertical shear $\partial\bar{u}/\partial z$, is believed to account for several important features of the observed Kelvin and Rossby-gravity waves. Together with thermal and perhaps mechanical dissipation, it is also an essential component of the models of the quasi-biennial oscillation mentioned in Chapter 8.

The most detailed treatments of the effects of a basic shear flow $\bar{u}(y, z)$ on the propagation of equatorial waves in the presence of dissipation necessarily involve numerical solution of Eqs. (4.7.1). For many purposes, though, a *WKBJ* approach (cf. Appendix 4A) is sufficient for gaining physical insight into the effects of shear. This theory is still quite complicated, and we shall only quote some basic results here.

For simplicity we consider the case where $\bar{u}$ depends on $z$ alone. The *WKBJ* assumption then requires that the basic shear is weak, in the sense that the height scale on which $\bar{u}$ varies is much greater than the vertical wavelength $2\pi m^{-1}$ of the waves under consideration. It also requires that

dissipative effects are small. These conditions can be formalized by introducing a small *WKBJ* parameter $\mu_w$, as in Section 4.5.4 and Appendix 4A.

At leading order in $\mu_w$, some of the results given above still hold locally, at each $z$. For example, upward-propagating Kelvin waves of absolute frequency $\omega$ and zonal wave number $k$ have a local vertical wavenumber $m(z)$ given by

$$\omega - k\bar{u}(z) = -Nk/m(z) > 0, \tag{4.7.23}$$

[cf. Eqs. (4.7.8a) and (4.7.10)] and a local vertical group velocity $c_g^{(z)}(z)$ given by

$$c_g^{(z)}(z) = Nk[m(z)]^{-2} = [\omega - k\bar{u}(z)]^2/Nk. \tag{4.7.24}$$

(The same formulas also hold when $N$ varies slowly with $z$.) In terms of the absolute zonal phase speed $c \equiv \omega/k$, these imply that Kelvin waves only exist in regions where $\bar{u}(z) < c$, since $k > 0$ by convention, and that the vertical wavelength $2\pi m^{-1}$ and $c_g^{(z)}$ both become small as $\bar{u}(z)$ approaches $c$, that is, as a wave approaches a critical level. Intuitively one expects the waves to become more and more susceptible to dissipation as the vertical group velocity decreases, and this can be confirmed theoretically, as mentioned below.

Similar results hold for Rossby-gravity waves: in particular, for the modes with westward phase speed with respect to the mean flow ($-\beta/k^2 < \omega - k\bar{u} < 0$), we have

$$m(z) = N[\omega - k\bar{u}(z)]^{-2}\{\beta + [\omega - k\bar{u}(z)]k\} \tag{4.7.25}$$

and

$$c_g^{(z)}(z) = -[\omega - k\bar{u}(z)]^3 N^{-1}\{2\beta + [\omega - k\bar{u}(z)]k\}^{-1}. \tag{4.7.26}$$

Once again the vertical wavelength and group velocity decrease as a critical level is approached, and the waves are expected to be strongly dissipated there.

At the next order in $\mu_w$, the effects of the weak shear and dissipation on the variation of wave amplitude appear. The amplitude factors $\hat{\Phi}_0$ and $\hat{v}_0$ of Eqs. (4.7.9) and (4.7.19) now vary slowly with height and time. The simplest way of determining this variation is to substitute the lowest-order solutions [e.g., Eqs. (4.7.9) or (4.7.19)] into the full form of the generalized Eliassen-Palm theorem (cf. Section 3.6) and integrate in $y$: see Appendix 4A for a general outline of this approach. This calculation confirms that the waves become strongly dissipated as $c_g^{(z)} \to 0$. It also gives the slow height dependence of the latitudinally integrated vertical component of the Eliassen-Palm flux $\int_{-\infty}^{\infty} F^{(z)}\, dy$, associated with the waves in question. This quantity depends, among other things, on the form and magnitude of the dissipation that is present in the middle atmosphere, and

is an essential ingredient for some of the models of the QBO to be presented in Chapter 8.

As with the *WKBJ* theory for midlatitude planetary waves, described in Section 4.5.4, the conditions for the strict validity of the results given in this section are frequently not satisfied. Nevertheless, the theory still provides a valuable qualitative, and often quantitative, model of the behavior of the observed equatorial waves in the middle atmosphere.

### *4.7.5 Observed Equatorial Waves*

The existence of Kelvin and Rossby-gravity waves in the equatorial lower stratosphere has been verified by a number of time-series analyses based on radiosonde data. The Kelvin waves are primarily of zonal wave number 1 and 2 with periods in the range 10–20 days. The Rossby-gravity waves are primarily of wave number 4, with westward phase propagation and with periods of 4–5 days. The observed characteristics of these modes are summarized in Table 4.1. In both cases the structures are in approximate

**Table 4.1**

Characteristics of the Dominant Observed Planetary-Scale Waves in the Equatorial Lower Stratosphere

| Theoretical description | Kelvin wave | Rossby-gravity wave |
|---|---|---|
| Discovered by | Wallace and Kousky (1968) | Yanai and Maruyama (1966) |
| Period (ground-based) $2\pi\omega^{-1}$ | 15 days | 4–5 days |
| Zonal wave number $s = ka\cos\phi$ | 1–2 | 4 |
| Vertical wavelength $2\pi m^{-1}$ | 6–10 km | 4–8 km |
| Average phase speed relative to ground | $+25\ \mathrm{m\ s^{-1}}$ | $-23\ \mathrm{m\ s^{-1}}$ |
| Observed when mean zonal flow is | Easterly (max. $\approx -25\ \mathrm{m\ s^{-1}}$) | Westerly (max. $\approx +7\ \mathrm{m\ s^{-1}}$) |
| Average phase speed relative to maximum zonal flow | $+50\ \mathrm{m\ s^{-1}}$ | $-30\ \mathrm{m\ s^{-1}}$ |
| Approximate observed amplitudes | | |
| $u'$ | $8\ \mathrm{m\ s^{-1}}$ | $2\text{–}3\ \mathrm{m\ s^{-1}}$ |
| $v'$ | 0 | $2\text{–}3\ \mathrm{m\ s^{-1}}$ |
| $T'$ | 2–3 K | 1 K |
| Approximate inferred amplitudes | | |
| $\Phi'/g$ | 30 m | 4 m |
| $w'$ | $1.5 \times 10^{-3}\ \mathrm{m\ s^{-1}}$ | $1.5 \times 10^{-3}\ \mathrm{m\ s^{-1}}$ |
| Approximate meridional scales $\left(\frac{2N}{\beta\lvert m\rvert}\right)^{1/2}$ | 1300–1700 km | 1000–1500 km |

agreement with theoretical expectations when doppler shifting by mean winds is considered.

As will be shown in Chapter 8, these waves are primarily responsible for driving the so-called quasi-biennial oscillation of the zonal mean winds in the lower stratosphere. The Kelvin waves appear in the data most prominently during periods when mean easterly winds exist at the base of the equatorial stratosphere. The zonal wind and temperature oscillations

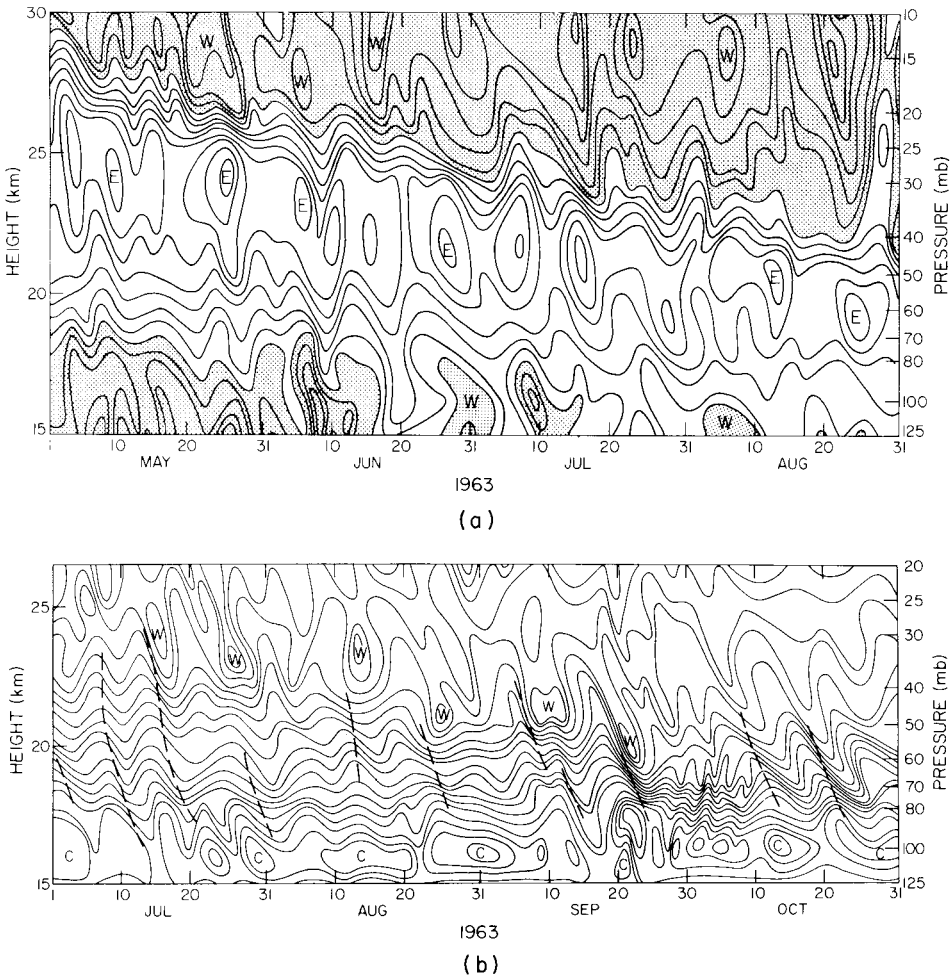


**Fig. 4.25.** Time-height sections for the equatorial lower stratosphere, showing evidence of Kelvin-wave activity. (a) Zonal wind and (b) temperature at Canton Island (3°S). Note the westerly phase of the QBO encroaching from upper levels in (a): see Chapter 8. [From Giu (1982).]

associated with the Kelvin wave can be quite dramatic, as indicated by the time-height sections of Fig. 4.25. The figure clearly indicates that the temperature fluctuations lag velocity fluctuations by one-fourth cycle and that phase propagates downward, consistent with Kelvin wave dynamics. Cross correlation with stations at other longitudes has confirmed the eastward propagation and long zonal wavelength.

It was noted in Section 4.7.3 that both the Kelvin and Rossby-gravity modes are thought to be generated by heating occurring in large-scale convective complexes (cloud clusters) in the equatorial zone. The model of Chang (1976) showed that randomly distributed sources most efficiently excite the longest zonal-scale Kelvin waves, and that the preferred vertical wavelength of the excited waves is about twice the vertical scale of the heat source, which from Fig. 4.24 is about 6 km for mature cloud clusters. This theory appears to account satisfactorily for the observed spectral distribution of Kelvin waves in the lower stratosphere.

A similar mechanism for frequency selection does not seem to operate for the Rossby-gravity mode. However, there is a rather distinct period of

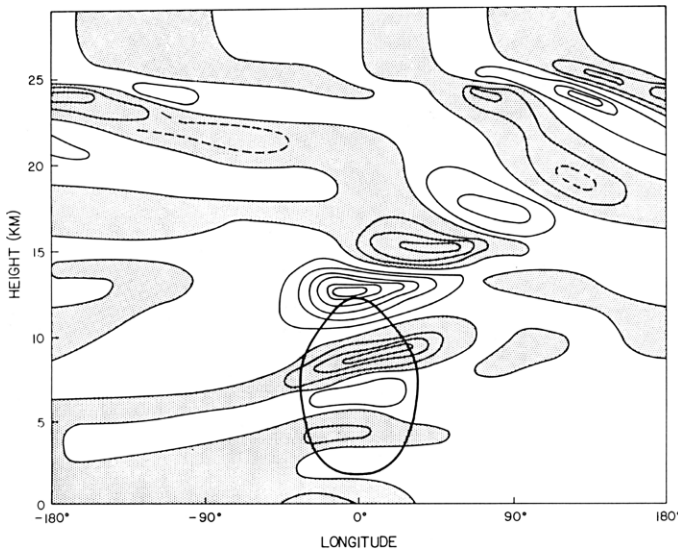


**Fig. 4.26.** Longitudinal-height section at the equator, showing the meridional wind disturbance excited by an antisymmetric heat source, at the time of maximum heating north of the equator. The mean zonal flow $\bar{u}(z)$ is westerly between 12 and 25 km altitude and easterly elsewhere. The heavy line encloses the region where the amplitude of the diabatic heating exceeds 4 K day$^{-1}$ at the latitude where it is a maximum. Isopleths are at 2-m s$^{-1}$ intervals, with shading indicating southerly winds. [After Holton (1972). American Meteorological Society.]

4–5 days in equatorial tropospheric convection. The model of Holton (1972, 1973) showed that a localized tropical heat source antisymmetric about the equator with a 5-day period can generate a Rossby-gravity response that is dominated by wave number 4 in the lower stratosphere. Figure 4.26, which shows the response to a standing heat source, also illustrates the eastward group velocity of the Rossby-gravity wave.

The relatively slow-moving Kelvin and Rossby-gravity modes observed in the lower stratosphere are effectively damped out by thermal dissipation by about the 10-mb level. Above that level the wave spectrum is dominated by more rapidly propagating Kelvin waves that were first reported in an analysis of rocketsonde data by Hirota (1978). Kelvin waves of several distinct frequency bands have been detected in the LIMS satellite data

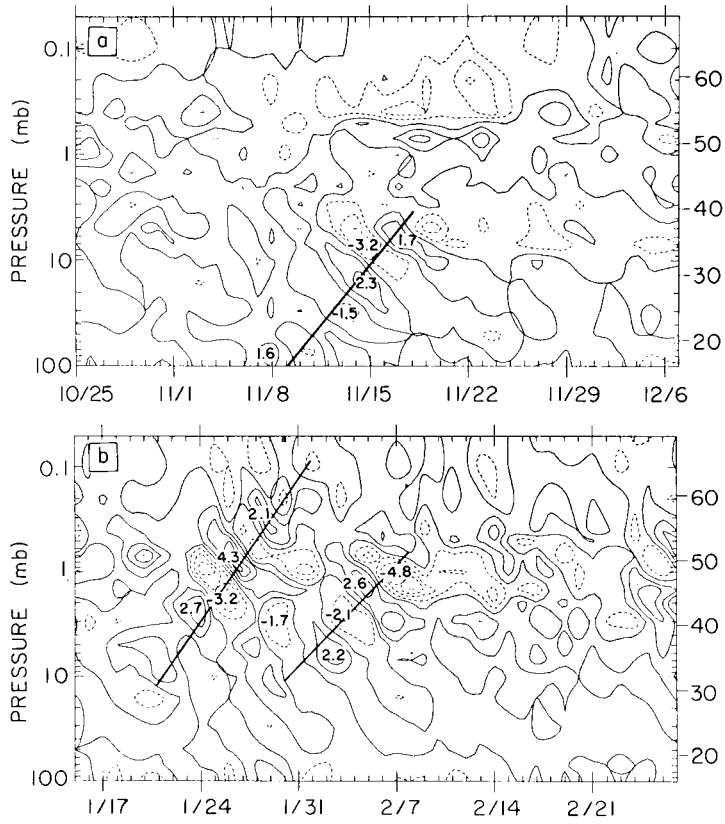


**Fig. 4.27.** Equatorial time–height sections of LIMS zonal wave 2 temperature at 0° longitude for the periods (a) October 25 to December 7, 1978, and (b) January 15 to February 27, 1979. Contour interval of 1 K. [After Coy and Hitchman (1984).]

(Salby *et al.*, 1984). These waves appear to be excited by isolated "events" in the troposphere and propagate into the middle atmosphere as distinct wave packets, as shown by the example of Fig. 4.27. Such waves are believed to provide the westerly accelerations necessary to maintain the semiannual mean zonal wind oscillation (see Section 8.5).

## Appendix 4A Ray-Tracing Theory and Wave Action in a Slowly Varying Medium

We present here a brief account of the application of "*WKBJ*" or "Liouville-Green" methods to problems involving the propagation of linearized waves in slowly-varying background states. We start by supposing that each disturbance quantity, such as the disturbance zonal velocity $u'$, can be written in the form

$$u' = \text{Re}\, \hat{u}(\mathbf{x}, t) \exp i\chi(\mathbf{x}, t) \tag{4A.1}$$

where $\mathbf{x} \equiv (x, y, z)$ and the phase $\chi$ is real. We *define* a local wave number vector $\mathbf{k} = (k, l, m)$ and frequency $\omega$ in terms of derivatives of $\chi$:

$$k \equiv \frac{\partial \chi}{\partial x}, \qquad l \equiv \frac{\partial \chi}{\partial y}, \qquad m \equiv \frac{\partial \chi}{\partial z}, \qquad \omega \equiv -\frac{\partial \chi}{\partial t}. \tag{4A.2}$$

We now make the crucial assumption that $\hat{u}$, $k$, $l$, $m$, and $\omega$, as well as the background medium, all vary much more slowly in time and space than does the phase. This can be formalized by requiring that their time and space scales are $O(2\pi\omega^{-1}\mu_w^{-1})$ and $O[2\pi(k^2 + l^2 + m^2)^{-1/2}\mu_w^{-1}]$, respectively, where $\mu_w$ is a small "*WKBJ* parameter," and thus are large compared with the wave period and wavelength, respectively. We also assume that a dispersion relation holds at each point in time and space:

$$\omega = \Delta(\mathbf{k}; \mathbf{x}, t). \tag{4A.3}$$

This relation follows, at leading order in $\mu_w$, from substitution into the linearized equations of motion [e.g., Eqs. (3.4.2)] of Eq. (4A.1) and similar expressions for the other disturbance variables; it thus contains dynamical information. Note that $\omega$ can depend on $\mathbf{x}$ both through the dependence of $\mathbf{k}$ on $\mathbf{x}$ and through the "explicit" $\mathbf{x}$ dependence of $\Delta$ due to $\mathbf{x}$ variations of the background state. (For example, if the background flow velocity depends on $z$, then $\Delta$ will contain explicit $z$ dependence.)

We define the group velocity $\mathbf{c}_g$ by

$$\mathbf{c}_g(\mathbf{k}; \mathbf{x}, t) = (c_g^{(x)}, c_g^{(y)}, c_g^{(z)}) = \left(\frac{\partial \Delta}{\partial k}, \frac{\partial \Delta}{\partial l}, \frac{\partial \Delta}{\partial m}\right), \tag{4A.4}$$

and introduce the time rate-of-change as measured by an observer moving

with the local group velocity:

$$\frac{d_g}{dt} \equiv \frac{\partial}{\partial t} + \mathbf{c}_g \cdot \nabla. \tag{4A.5}$$

An important set of identities follows from the definitions of Eq. (4A.2) using relations like $\partial^2\chi/\partial x\,\partial t \equiv \partial^2\chi/\partial t\,\partial x$: for example,

$$\frac{\partial k}{\partial t} = -\frac{\partial \omega}{\partial x}, \qquad \frac{\partial k}{\partial y} = \frac{\partial l}{\partial x}, \qquad \frac{\partial k}{\partial z} = \frac{\partial m}{\partial x}. \tag{4A.6}$$

Thus

$$\frac{d_g k}{dt} \equiv \frac{\partial k}{\partial t} + \mathbf{c}_g \cdot \nabla k = -\frac{\partial \omega}{\partial x} + \frac{\partial \Delta}{\partial k}\frac{\partial k}{\partial x} + \frac{\partial \Delta}{\partial l}\frac{\partial l}{\partial x} + \frac{\partial \Delta}{\partial m}\frac{\partial m}{\partial x}, \tag{4A.7}$$

using Eqs. (4A.5), (4A.6), and (4A.4); but from Eq. (4A.3),

$$\frac{\partial \omega}{\partial x} = \frac{\partial \Delta}{\partial k}\frac{\partial k}{\partial x} + \frac{\partial \Delta}{\partial l}\frac{\partial l}{\partial x} + \frac{\partial \Delta}{\partial m}\frac{\partial m}{\partial x} + \frac{\partial \Delta}{\partial x} \tag{4A.8}$$

using the chain rule, and so Eqs. (4A.7) and (4A.8) imply

$$\frac{d_g k}{dt} = -\frac{\partial \Delta}{\partial x}. \tag{4A.9a}$$

In a similar manner it can be shown that

$$\frac{d_g l}{dt} = -\frac{\partial \Delta}{\partial y}, \qquad \frac{d_g m}{dt} = -\frac{\partial \Delta}{\partial z}, \qquad \frac{d_g \omega}{dt} = \frac{\partial \Delta}{\partial t}. \tag{4A.9b,c,d}$$

Thus the rate-of-change, following the group velocity, of the local wave number or frequency depends on the "explicit" space or time variation of $\Delta$ due to inhomogeneities of the background state.

We now define a *ray* as the trajectory $\mathbf{x}(t)$ of a point moving with the local group velocity, that is,

$$\frac{d_g \mathbf{x}}{dt} = \mathbf{c}_g[\mathbf{k}(\mathbf{x}(t), t); \mathbf{x}(t), t]. \tag{4A.10}$$

Equations (4A.9) and (4A.10) are called the *ray-tracing equations*: given the dispersion relation [Eq. (4A.3)] and appropriate initial conditions on $\mathbf{x}$ and $\mathbf{k}$, they can in principle be solved for the ray paths and the variation of local wave number and frequency along the rays. Physically, Eq. (4A.10) can be regarded as giving the trajectory of a "wave packet" whose wave number $\mathbf{k}$ and frequency $\omega$ vary according to Eq. (4A.9).

Examples of the use of ray-tracing theory are discussed in Section 4.5.4 for planetary waves in a zonal shear flow $\bar{u}(y, z)$ and mentioned in Section 4.6.2 for internal gravity waves in a zonal shear flow $\bar{u}(z)$; the latter case is particularly amenable to analytical treatment (e.g., Bretherton, 1966b). Further details of the technique are given, for example, by Lighthill (1978) and Gill (1982).

The ray-tracing equations give no information about the amplitude variation of wave packets; for this purpose a more complex theory is required, and we shall only quote the main results here. For simplicity, we specialize to the case of waves of slowly varying amplitude in a basic unforced flow $[\bar{u}(y, z), 0, 0]$ that is zonal, independent of $x$ (so that $\partial\Delta/\partial x = 0$) and $t$, and slowly varying in $y$ and $z$. Since this flow is zonal, unforced, and $x$-independent, the generalized Eliassen-Palm theorem [Eq. (3.6.2)] holds; using the slowly varying properties of the waves and mean flow it can be shown [using methods analogous to those of Andrews and McIntyre (1976a,b, 1978c)] that

$$\mathbf{F} = \mathbf{c}_g A \tag{4A.11}$$

to leading order in $\mu_w$. (A special case of this result, for planetary waves, is mentioned in Section 4.5.5.) It can also be shown that

$$A = -k\left(\frac{E}{\omega - k\bar{u}}\right) \tag{4A.12}$$

to leading order in $\mu_w$, where $E$ is the wave-energy density $\frac{1}{2}\rho_0(\overline{u'^2} + \overline{v'^2} + \Phi_z'^2/N^2)$ [cf. Eq. (3.6.3)]. The expression $E/(\omega - k\bar{u})$ is called the *wave-action density*; using Eqs. (3.6.2), (4A.11), (4A.12), and (4A.9a), together with the fact that $\partial\Delta/\partial x = 0$ here, one obtains the wave-action equation

$$\frac{\partial}{\partial t}\left(\frac{E}{\omega - k\bar{u}}\right) + \nabla \cdot \left(\frac{\mathbf{c}_g E}{\omega - k\bar{u}}\right) = \text{nonconservative effects} + O(\alpha^3) \tag{4A.13}$$

for slowly varying waves (Bretherton and Garrett, 1968; Andrews and McIntyre, 1978c). (Here $\alpha \ll 1$ is a dimensionless wave amplitude, as in Chapter 3.) Equation (4A.13) can be rewritten

$$\frac{d_g}{dt}\left(\frac{E}{\omega - k\bar{u}}\right) + \left(\frac{E}{\omega - k\bar{u}}\right)\nabla \cdot \mathbf{c}_g = \text{nonconservative effects} + O(\alpha^3)$$

and, if the nonconservative terms are known, this can be used to find the variation of wave action (and thence of wave energy and other measures of wave amplitude) along a ray, to $O(\alpha^2)$. Note that, in general, information on a bundle of adjacent rays is required for calculation of $\nabla \cdot \mathbf{c}_g$ here.

For equatorial waves (Sections 4.7 and 8.3) the assumption of slow variation of wave amplitude in $y$ is no longer valid; however, in the case where $\bar{u}$ depends on $z$ alone it can be shown that

$$\int F^{(z)}\, dy = c_g^{(z)} \int A\, dy, \tag{4A.14}$$

where the integrals are taken from $-\infty$ to $\infty$. From Eq. (3.6.2) it then follows that

$$\frac{\partial}{\partial t}\int A\, dy + \frac{\partial}{\partial z}\left(c_g^{(z)} \int A\, dy\right) = -2\gamma(z) \int A\, dy \tag{4A.15}$$

to $O(\alpha^2)$, where $2\gamma(z) \equiv -\int D\, dy / \int A\, dy$ and $D$ is the nonconservative term in Eq. (3.6.2). If $X'$, $Y'$, $Q'$ [see Eq. (3.4.2)] represent dissipative effects, it can be shown that $\gamma(z)$ is a positive inverse relaxation time. [For example, if $X' = -\gamma_1 u'$, $Y' = -\gamma_2 v'$, $Q' = -\gamma_3 \theta'$, then $\gamma$ is a weighted mean of $\gamma_1$, $\gamma_2$, $\gamma_3$ at each $z$ whose precise form generally depends on the detailed equatorial wave solutions: cf. Andrews and McIntyre (1976b); however, if $\gamma_1 = \gamma_2 = \gamma_3$, then $\gamma = \gamma_1$.] For steady waves, Eqs. (4A.14) and (4A.15) give

$$\int F^{(z)}\, dy = \int F^{(z)}\, dy \bigg|_{z=z_0} \exp\left\{-\int_{z_0}^{z} \frac{2\gamma(z')\, dz'}{c_g^{(z)}(z')}\right\} \tag{4A.16}$$

[cf. Eqs. (8.3.1) and (8.3.6)]. Note that the exponential decay factor in Eq. (4A.16) tends to be enhanced by small values of the vertical group velocity $c_g^{(z)}$, implying strong attenuation of the waves: see Sections 4.7.4 and 8.3.2 for some possible consequences of this result.

## References

4.1. General treatments of linear waves in rotating, stratified fluids are given in many texts: for example Gill (1982) and Pedlosky (1979) both discuss a variety of waves of atmospheric and oceanic interest. Lighthill (1978) gives a thorough account of the general principles of wave propagation in fluids, and includes several geophysical applications.

4.2. The material summarized in this section is treated in more detail by Chapman and Lindzen (1970), for example. Some mathematical properties of Hough functions are given by Lindzen (1971); questions of their completeness are discussed by Holl (1970).

4.3. A basic source on atmospheric tidal theory and observation is Chapman and Lindzen (1970). Recent reviews include Lindzen (1979), Forbes and Garrett (1979) and Forbes (1984). Rocket observations are discussed by Reed (1972) and Groves (1976). Radar observations of mesospheric tides are given by Manson *et al.* (1985). Recent satellite measurements of middle atmosphere tides, and comparisons with

simple theory, are presented by Brownscombe *et al.* (1985). The simple, approximate theory for the vertical structure of the semidiurnal tide given near the end of Section 4.3.3 follows Green (1965). The contributions of latent heating to the excitation of the semidiurnal tide are investigated by Hamilton (1981a).

4.4. Recent reviews of the theory and observation of free traveling planetary waves are given by Madden (1979), Walterscheid (1980), and Salby (1984). The "ducted" mode peaking near the stratopause was investigated theoretically by Salby (1979, 1980). The sensitivity of the 5-day wave to the background wind structure was studied by Geisler and Dickinson (1976). Observational evidence for the excitation of the 5-day wave by tropical latent heating is presented by Hamilton (1985).

4.5. The theory of tropospherically forced planetary waves propagating into the middle atmosphere was initiated by Charney and Drazin (1961) and is to be found in several standard texts. The calculation of parcel orbits in Section 4.5.3 follows Matsuno (1980). Fundamental work on the propagation of planetary waves in basic flows depending on latitude and height, including consideration of critical lines and ray-tracing, was performed by Dickinson (1968). The propagation of planetary waves in mean flows $\bar{u}(y)$, containing only meridional shear, is considered, for example, by Boyd (1982a,b).

4.6. Fritts (1984) gives an excellent review of middle atmosphere gravity wave observations and theory. Radar observations are discussed in some detail by Vincent (1984). For the Boussinesq approximation see, for example, Gill (1982). The effects of radiative damping on gravity-wave breaking are examined by Fels (1984, 1985) and Holton and Zhu (1984). The possible importance of inertio-gravity waves in the middle atmosphere is considered by Dunkerton (1984). Evidence for inertio-gravity waves in rocketsonde winds is presented by Hirota and Niki (1985).

4.7. The foundations of the modern theory of atmospheric equatorial waves were laid by Matsuno (1966). Further details on the *WKBJ* theory of Section 4.7.4 are given by Lindzen (1971, 1972), Andrews and McIntyre (1976a,b), and Boyd (1978a,b).